MicroBooNE: The Search For The Low Energy Excess

David Kaleko

Submitted in partial fulfillment of the
requirements for the degree
of Doctor of Philosophy
in the Graduate School of Arts and Sciences

COLUMBIA UNIVERSITY

2017

ABSTRACT

MicroBooNE: The Search For The Low Energy Excess

David Kaleko

The abstract goes here. The abstract goes here. The abstract goes here. The abstract goes here. The abstract goes here. The abstract goes here. The abstract goes here. The abstract goes here. The abstract goes here. The abstract goes here. The abstract goes here. The abstract goes here.

Table of Contents

1 Introduction **1**

2 Neutrinos, Neutrino Oscillations, and Sterile Neutrinos **3**

2.1 Introduction to Neutrinos 3

2.2 Neutrino Oscillations 3

2.2.1 Neutrino Measurements 3

2.3 LSND Observation and Sterile Neutrino 3

2.4 Antineutrino Disappearance 3

3 The MicroBooNE Detector **5**

3.1 MicroBooNE Detector Section 5

3.1.1 MicroBooNE Detector Subsection 5

4 The Booster Neutrino Beam **7**

4.1 Beam Section 1 7

4.1.1 Beam Subsection 1.1 7

5 Low Energy Excess Sensitivity Studies **9**

5.1 Low Energy Excess Overview and Motivation 9

5.1.1 Introduction 9

5.1.2 LSND Observation 10

5.1.3 The MiniBooNE Experiment 10

5.1.4 MicroBooNE In The Context of the Low Energy Excess 19

5.2 Monte Carlo Simulation 20

5.2.1 Simulated Background Samples 20
5.2.2 Reconstruction 21
5.3 Event Selection 23
5.3.1 Electron/Photon Separation Algorithm 24
5.3.2 Signal Selection Algorithm 28
5.3.3 Energy Reconstruction 35
5.4 Backgrounds 35
5.4.1 Background Topologies 35
5.4.2 Background Normalization 40
5.4.3 Analysis Cuts and Results 40
5.5 MiniBooNE Low Energy Excess Signal Modeling In MicroBooNE 43
5.5.1 Sensitivity Results 45

6 Kaon Production Studies **51**
6.1 Kaon Production Section 1 51
6.2 Kaon Production Section 2 51
6.2.1 kaon production subsection 2.1 51

7 Multiple Coulomb Scattering **53**
7.1 MCS theory 53
7.2 MCS algorithm 53
7.3 MCS measurements on contained tracks in data 53
7.4 MCS measurements on exiting tracks in simulation 53

8 Conclusions **55**

I Appendices **57**

A Appendix title **59**
A.1 Sample section 59
A.1.1 Sample subsection 59
A.1.2 Sample subsubsection 60

A.2 Sample section 60
A.2.1 Sample subsection 60

II Bibliography **61**

Bibliography **63**

List of Figures

5.1 *The MiniBooNE detector enclosure (left) and a cut-away drawing (right) of the detector showing the distribution of PMT's in the signal and veto regions.* 11

5.2 *A schematic of the pattern Cherenkov light from different particles would make projected onto the inner walls of the MiniBooNE detector. Top is a muon track (a filled-in ring), middle is an electron (a fuzzy ring), bottom is a photon that pair-produces and creates two fuzzy rings.* 13

5.3 *Feynman diagrams of the charged-current quasi-elastic (CCQE) interaction channel for ν_e, ν_μ, $\overline{\nu_\mu}$, and $\overline{\nu_e}$ (clockwise from the top left). ν_e CCQE is the signal channel for the MiniBooNE oscillation analysis.* 14

5.4 *The E_ν^{QE} distribution for MiniBooNE data (points with statistical errors) and and backgrounds (histogram with systematic errors).* 16

5.5 *The MiniBooNE event excess as a function of E_ν^{QE}. Also shown are the expectations from the best oscillation fit and from neutrino oscillation parameters in the LSND allowed region. The error bars include both statistical and systematic errors.* 17

5.6 *A preliminary attempt to scale the MiniBooNE backgrounds and excess to the MicroBooNE both under the assumption that the excess is due to an electron-like event (left) or under a photon-like event (right). Stacked histograms show the expected background. Error bars indicate statistical uncertainty. The number of signal events, scaled from MiniBooNE for neutrino flux and fiducial volume, is the same in both plots. Both plots assume $6.6 \times 10^2 0$ POT for the MicroBooNE 60 ton fiducial mass.* 20

5.7 *AlgoEMPart training results on perfect reconstructed electron showers and on perfect reconstructed photon showers as described in Section 5.3.1.1: 1D landau + gaussian fit to dE/dx.* 26

5.8 *The same plot as shown in Figure 5.7, but zoomed in along the y-axis to show the compton peak in the photon sample, as well as the pileup of very low dE/dx values for photons (due to soft compton scatters as described in Section 5.2.2.1).* 27

5.9 *AlgoEMPart: Computed 1D likelihood vs dE/dx: red is photon, blue is electron. How the likelihood is computed is described in Section 5.3.1.1.* 28

5.10 *AlgoEMPart training results on perfect reconstructed electron showers as described in Section 5.3.1.1: Radiation length fit to single electron showers. Note the poor quality of the fit as the electron conversion distance for "perfect reconstruction" does not follow an exponential distribution; all conversion distances are below 0.3 centimeters.* 29

5.11 *AlgoEMPart training results on perfect reconstructed photon showers as described in Section 5.3.1.1: Radiation length fit to single photon showers.* . . 30

5.12 *AlgoEMPart: Computed 1D likelihood vs conversion distance (integrated over all energies): red is photon, blue is electron. How the likelihood is computed is described in Section 5.3.1.1.* 30

5.13 *AlgoEMPart training results on perfect reconstructed electron and photon showers as described in Section 5.3.1.1 integrated over all energies: 2D likelihood distribution (radiation length vs. dE/dx). Low values of likelihood (purple) correspond to photon-like, high values (red) correspond to electron-like.* 31

5.14 *A flowchart depicting decisions the algortihm makes for each primary, non-cosmic shower. If the algorithm gets to the bottom of the flowchart, that shower was determined to be from a $\nu_e CC$ interaction, and a ν_e particle is created.* 32

5.15 *Schematic cartoons indicating how the signal selection algorithm makes decisions determining if two reconstructed showers are correlated, and if a reconstructed shower is correlated with a reconstructed track (as described in Figure 5.14).* 33

5.16 *Reconstructed neutrino energy as described in Section 5.3.3 versus true neutrino energy. This plot was made from "perfect reconstruction" objects in correctly identified ν_eCCQE events after all final analysis cuts were placed.* . 36

5.17 *A neutrino energy resolution and bias plot. This is created by binning Figure 5.16 in true neutrino energy and making a distribution of (Reco Energy - True Energy)/(True Energy). For each bin, the mean (red) and standard deviation (blue) are plotted in the above figure. This plot was made from "perfect reconstruction" objects in correctly identified ν_eCCQE events after all final analysis cuts were placed.* 37

5.18 *The backgrounds to the ν_eCCQE appearance search in MicroBooNE. The event selection is described in Section 5.3, the background topologies described in Section 5.4.1, the relative normalization between samples described in Section 5.4.2, and the energy reconstruction described in Section 5.3.3.* 42

5.19 *The computed distribution of u_z (how foward-going the event is) vs. E_{vis} for N = 1000 times the MiniBooNE low energy excess (raw) events.* 45

5.20 *The backgrounds to the ν_eCCQE appearance search in MicroBooNE with scaled signal drawn. The event selection is described in Section 5.3, the background topologies described in Section 5.4.1, the relative normalization between samples described in Section 5.4.2, and the energy reconstruction described in Section 5.3.3. The scaled signal is described in Section 5.5.* . . 46

5.21 *The backgrounds to the ν_eCCQE appearance search in MicroBooNE with scaled signal drawn. The event selection is described in Section 5.3, the background topologies described in Section 5.4.1, the relative normalization between samples described in Section 5.4.2, and the energy reconstruction described in Section 5.3.3. The scaled signal is described in Section 5.5. Here the shower reconstrution efficiency has been decreased from the "perfect reconstruction" value of 100% to 85% to emulate possible realistic shower reconstruction efficiencies.* 47

Acknowledgments

The acknowledgments go here.

Dedication text

Chapter 1

Introduction

The introduction will be brief, and will introduce the reader to the document. It will outline the flow of the thesis: start with a description of neutrinos and some basic neutrino theory, then describe the MicroBooNE detector, then describe the BNB, then dive in to the Low Energy Excess section which contains description of LSND, description of MiniBooNE, description of the analysis in MicroBooNE, the sensitivity results in MicrobooNE. That section ends with describing how the flux systematic on intrinsuc nues from kaon decay (an important background in the LEE search) can be improved with an in-situ measurement of numus from kaons. Then comes the numu-from-kaon section, which references the importance of multiple Coulomb scattering and I will copy/paste the JINST publication in there. Then there will be a short conclusions/summary section, followed by any appendices which are needed.

Chapter 2

Neutrinos, Neutrino Oscillations, and Sterile Neutrinos

2.1 Introduction to Neutrinos

2.2 Neutrino Oscillations

2.2.1 Neutrino Measurements

2.3 LSND Observation and Sterile Neutrino

2.4 Antineutrino Disappearance

Chapter 3

The MicroBooNE Detector

3.1 MicroBooNE Detector Section

3.1.1 MicroBooNE Detector Subsection

Chapter 4

The Booster Neutrino Beam

4.1 Beam Section 1

4.1.1 Beam Subsection 1.1

Chapter 5

Low Energy Excess Sensitivity Studies

5.1 Low Energy Excess Overview and Motivation

5.1.1 Introduction

The purpose of this chapter is to describe the MicroBooNE analysis centered around measuring the observed low energy excess as seen by its predicessor experiment, MiniBooNE. This chapter begins with a historical motivation for this analysis by describing the LSND experiment which first observed an excess of $\overline{\nu}_e$ in a $\overline{\nu}_\mu$ beam. Then, a detailed description of the MiniBooNE experiment (detector and analysis) is provided, which observed an unexplained excess of electron-like events in the neutrino energy region between 200 to 475 MeV.

With historical context in perspective, this chapter then discusses an analysis conducted which determines the sensitivity of the previously described MicroBooNE detector to measure the same signal as MiniBooNE, assuming that signal originated from an excess of beam-induced ν_e interactions. This discussion covers the signal modeling which comes from MiniBooNE published data releases, the event selection and background mitigation techniques in MicroBooNE, and ultimately the expected sensitivity to measure such a signal.

5.1.2 LSND Observation

In 2001, the Liquid Scintillator Neutrino Detector (LSND) collaboration published an observation of excess events consistent with $\overline{\nu}_e$ interactions above the expected background in an $\overline{\nu}_\mu$ beam at the Los Alamos Neutron Science Center [Aguilar-Arevalo and others, 2001]. Given the $\frac{L}{E}$ ($\approx \frac{30m}{40MeV}$) for this measurement, the excess disagreed with previous measurements of neutrino mixing angles and Δm^2 values in the three neutrino model. The LSND excess corresponded to a Δm^2 of approximately 1 eV^2, significantly higher than previously measured values of Δm^2_{12} and Δm^2_{23}. One explanation for this drastically different Δm^2 value is the existance of potential additional "sterile" neutrino states, which must not interact weakly given the Z- boson decay width constrains the number of weakly interacting neutrino states to three.

To test the LSND result, the MiniBooNE experiment was designed. It would measure ν_e interactions in a primarily ν_μ beam, with a similar $\frac{L}{E}$ ($\approx \frac{500m}{700MeV}$). The beam could also be modified to produce primarily $\overline{\nu}_\mu$ and MiniBooNE would therefore measure $\overline{\nu}_e$.

5.1.3 The MiniBooNE Experiment

5.1.3.1 The MiniBooNE Detector and Monte Carlo Simulation

The MiniBooNE detector [Aguilar-Arevalo and others, 2009a] consists of a spherical tank located 541 meters downstream of the BNB neutrino production target, with diameter of 12.2 meters filled with 818 tons of mineral oil underneath at least 3 meters of earth overburden as shown in Figure 5.1. As seen in the figure, there exists an opaque barrier separating a veto region and a signal region. The walls of the signal region are painted black to reduce re-scattering of light and are instrumented with 1280 8-inch photomultiplier tubes (PMTs), most of which were reused from the LSND experiment. In the signal region, the photocathode coverage is 11.8%. This region is intended to identify beam neutrino interactions happening within it; the PMTs face radially inwards. The veto region is 35 cm thick and is instrumented with 240 PMTs which face tangent to the detector radius and its purpose is to reject backgrounds coming from outside of the detector (cosmics, which have a rate at the detector location of about 10 kHz). The inner surface of the veto region is coated in

a reflective paint. The efficiency for rejecting cosmic ray muons with the outer veto region was measured to be 99.99%.

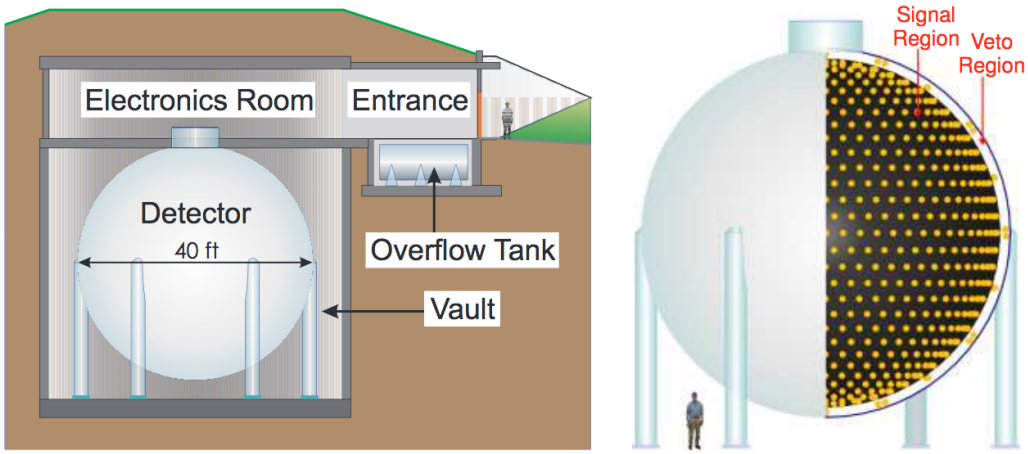

Figure 5.1: *The MiniBooNE detector enclosure (left) and a cut-away drawing (right) of the detector showing the distribution of PMT's in the signal and veto regions.*

The detection method of the MiniBooNE experiment is based primarily on Cherenkov light. The mineral oil within the signal region acts as the neutrino target material. The majority of final state particles exiting neutrino interactions at neutrino energies from the BNB are produced above Cherenkov threshold. These particles produce Cherenkov light which is detected by the PMTs lining the signal region of the detector. Reconstructing the pattern this light projects onto the walls of the signal region allows for some particle identification abilities.

Thie mineral oil used in MiniBooNE is Marcol 7 Light Mineral Oil (CH_2). While the oil has lower density than water (a common material choice for Cherenkov detectors) and therefore smaller probability of a neutrino interacting within the detector, the other benefits outweigh this downside. The oil has good light transmission throughout the wavelength range of 320 nm to 600 nm, relatively large refractive index (1.47, greater than water at 1.33), and its long extinction length of greater than 20 m for 420 nm light. This extinction length allows for loss of no more than 25% of light generated by a neutrino interaction at

the center of the detector. Additionally, the Cherenkov threshold is lower than that of water for the final state particles of interest (electrons, pions, muons, protons), allowing for the measurement of lower energy particles.

The PMTs have a wavelength dependent efficiency with a peak at 390 nm, with half that efficiency at 315 and 490 nm. They are operated at +2000 V which results in a gain of approximately 1.6×10^7. They have an intrinsic time resolution on the order of 1 ns, which is the dominant contribution to the final time resolution in the final PMT data after readout through data acquisition (DAQ) electronics. The DAQ reads out a PMT when the charge signal corresponds to more than 0.1 photoelectrons (PE). The deadtime between successive PMT readouts is on the order of 250 ns after the first readout began. PMT charge and timing information is stored in intervals of 200 μs following any trigger signal. The trigger signal of interest for this analysis is the beam trigger which is induced by the BNB accelerator clock such that the DAQ begins readout 5 μs before each beam spill.

The detector is calibrated *in situ* primarily from cosmic ray muons. Within the detector are six optically sealed scintillator cubes. Incoming muons are tagged with a muon hodoscope above the detector with angular resolution better than 2 degrees. Those muons that stop within one of the scintillation cubes have well defined energy (in the 100-800 MeV range), as the stopping power of muons in mineral oil is well known, and therefore provide an energy calibration source. Additionally, the outgoing electrons from stopping muon decay (Michel electrons) have a well known endpoint of around 50 MeV and therefore serve as an electron energy calibration source at that energy. Through-going muons are also used as an energy calibration source at higher energies (above 1 GeV). Additional calibration sources include a laser system built into the detector, and reconstructed π^0 masses (with peak energy at 135 MeV).

5.1.3.2 MiniBooNE Event Selection and Observed Excess

Different final state particles exiting a neutrino interaction in the MiniBooNE signal volume create different patterns of Cherenkov light read out by the PMTs. Figure 5.2 [Karagiorgi,

2010] shows how these patterns differ for different common kinds of final state particles (muons, electrons/photons, and neutral pion decays). A muon track produces a crisp, filled-in ring of Cherenkov light, while an electron or photon produces a more fuzzy, hollow ring. A neutral pion decay will result in two photons. By reconstructing these patterns in the PMT data read out from a triggered event in MiniBooNE, the flavor and energy of the interacting neutrino can be determined. With this kind of detection technique it is important to note that a single photon signal is indistinguishable from that of a single electron signal, an important ingredient to the ultimate ambiguity of the observed low energy excess in MiniBooNE.

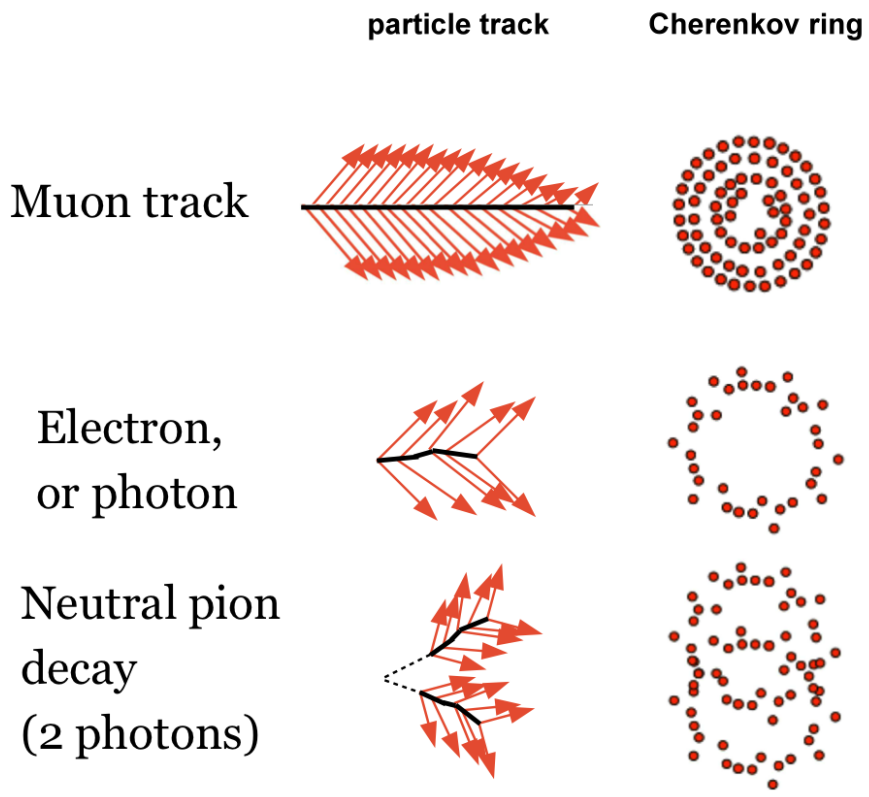

Figure 5.2: *A schematic of the pattern Cherenkov light from different particles would make projected onto the inner walls of the MiniBooNE detector. Top is a muon track (a filled-in ring), middle is an electron (a fuzzy ring), bottom is a photon that pair-produces and creates two fuzzy rings.*

The topology of interest in the MiniBooNE oscillation search is that of charged-current quasi-elastic (CCQE) interactions, shown in Figure 5.3. This interaction channel is the dominant one in the neutrino energy range of the BNB, around 1 GeV E_ν. In a ν_l CCQE interaction (where l is the neutrino flavor), a lepton of flavor l is produced, along with a proton. The single outgoing lepton is the characteristic event signature for which MiniBooNE searches.

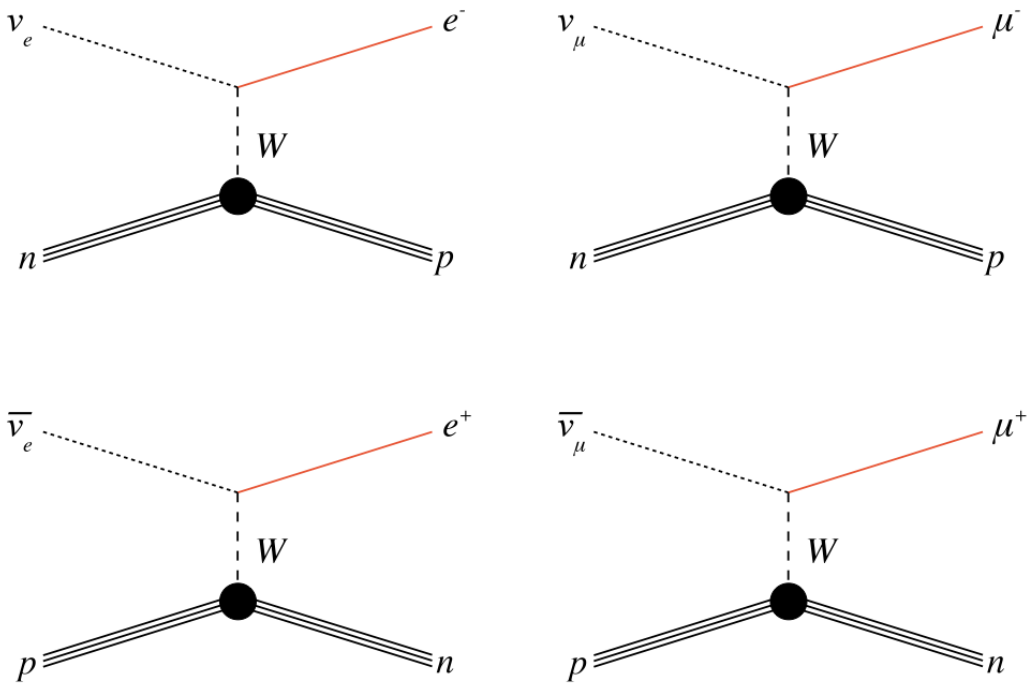

Figure 5.3: *Feynman diagrams of the charged-current quasi-elastic (CCQE) interaction channel for ν_e, ν_μ, $\overline{\nu_\mu}$, and $\overline{\nu_e}$ (clockwise from the top left). ν_e CCQE is the signal channel for the MiniBooNE oscillation analysis.*

In order to select ν_e^{CCQE} events, cuts are placed to mitigate backgrounds. The most powerful rejection comes from requiring the events occur within the beam timing window. Two additional cuts are used that require there be more activity within the signal volume than the outer veto volume, a signature characteristic of beam related neutrino events. These pre-cuts achieve more than a 99.99% rejection of beam unrelated backgrounds.

In order to reconstruct events, MiniBooNE uses a maximum likelihood fitting algorithm leveraging properties of charged particle tracks inferred from measured charges and times on the PMTs. The likelihoods to different event hypothesis are used to classify each event as a signal ν_e CCQE event, or as a background process like ν_μ CCQE and NC π^0 production. Note that MiniBooNE cannot differentiate between a μ^+ and a μ^-, or e^+ and e^- so discrimination between neutrino and antineutrino on an event-by-event basis is impossible.

Assuming CCQE kinematics, the incident neutrino energy is reconstructed with knowledge of the outgoing lepton energy (E_l) and scattering angle (θ_l). In MiniBooNE specifically, the struck nucleon is assumed to be at rest, so the incident neutrino energy E_ν^{CCQE} is given by:

$$E_\nu^{CCQE} = \frac{2m_n E_l + m_p^2 - m_n^2 - m_l^2}{2(m_n - E_l + \cos\theta_l \sqrt{E_l^2 - m_l^2})} \tag{5.1}$$

where m_n, m_p, m_l are the masses of the neutron, proton, and lepton respectively, and θ_l is the scattering angle of the outgoing lepton with respect to the (known) beam neutrino direction.

With the described reconstruction methods and energy definition, the MiniBooNE published results [Aguilar-Arevalo and others, 2009b] for the ν_e appearance search in neutrino mode running are shown in Figure 5.4. There is clearly a statistically significant excess of events below E_ν^{CCQE} of 475 MeV. Note that besides the irriducible intrinsic ν_e backgrounds, the dominant background in the excess region is π^0 MID (red). In a π^0 MID event event, a π^0 is created in the neutrino interaction and its subsequent immediate decay into two photons mimics a the ν_e CCQE signature (either one photon escapes, or rings overlap). Another important background is $\Delta \to N\gamma$ (brown). Recall that both of these backgrounds arise from MiniBooNE's inability to distinguish electrons from photons.

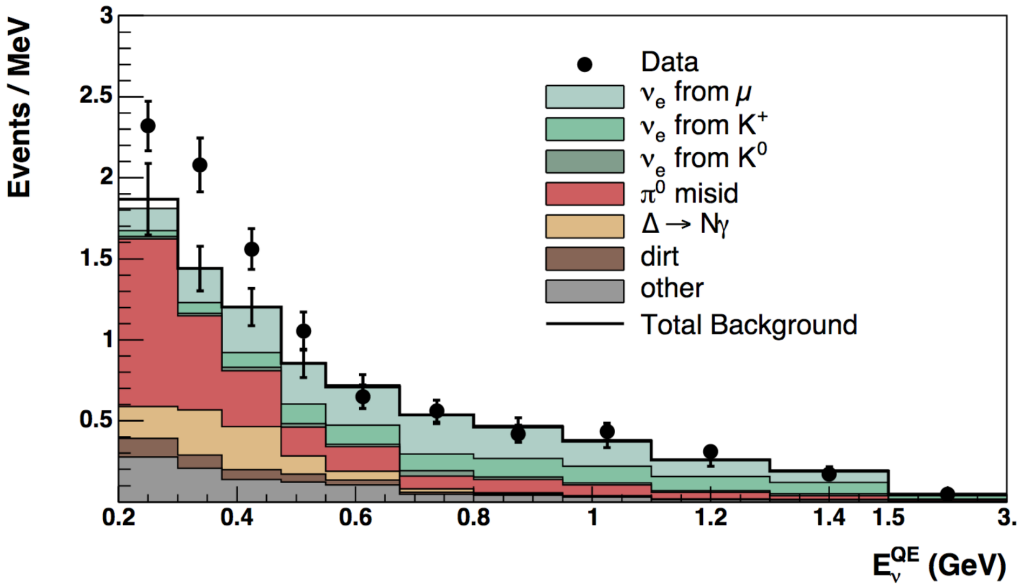

Figure 5.4: *The E_ν^{QE} distribution for MiniBooNE data (points with statistical errors) and and backgrounds (histogram with systematic errors).*

5.1.3.3 Proposed Low Energy Excess Sources

Shown in Figure 5.5 is the MiniBooNE neutrino mode excess (data - expected background) with oscillation fits with parameters constrained to be in the LSND allowed region. The parameters in the LSND allowed region are ruled out at the 95% confidence level if the data are fit with $E_\nu^{CCQE} > 475$ MeV.

Given MiniBooNE's inability to distinguish electrons from photons, the origin of this excess is either a mis-estimation of one of the backgrounds, or some sort of new physics. The former is unlikely the case because MiniBooNE makes many *in situ* measurements that allow for the constraining of these backgrounds. The neutral current induced backgrounds (NC π^0, $\Delta \rightarrow N\gamma$, and dirt) are constrained by such measurements. Measurements constraining these backgrounds are described in the following paragraphs.

The NC π^0 rate in MiniBooNE is measured by selecting events with reconstructed mass near the π^0 mass. This obtains a $> 90\%$ pure sample of NC π^0 interactions which is

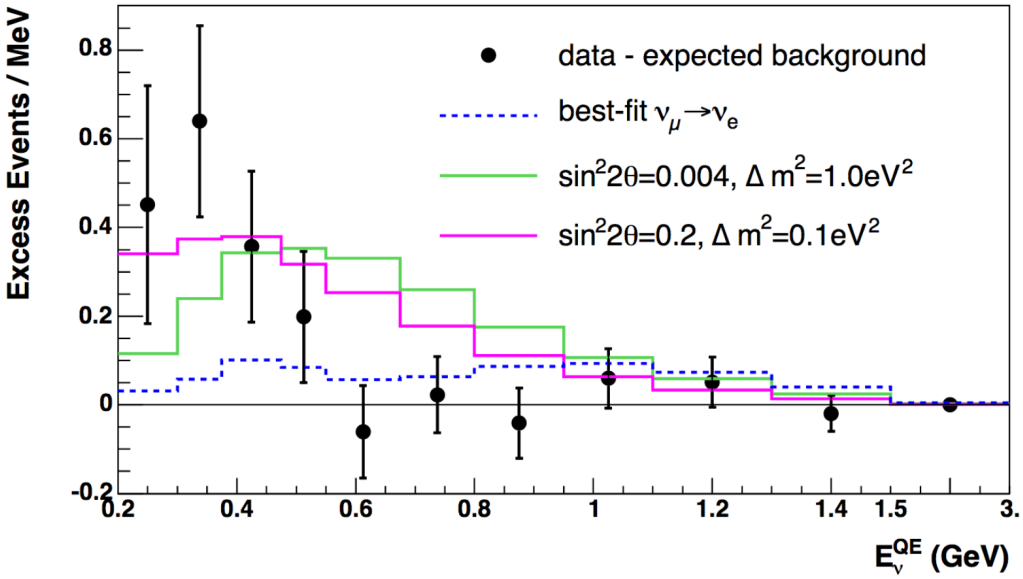

Figure 5.5: *The MiniBooNE event excess as a function of* E_ν^{QE}*. Also shown are the expectations from the best oscillation fit and from neutrino oscillation parameters in the LSND allowed region. The error bars include both statistical and systematic errors.*

compared to simulation to obtain a correction function in order to bring the simulated distribution in agreement with data. This same correction function is applied to NC π^0 events that are backgrounds in the ν_e appearance analysis. This correction function increases the NC π^0 background by less than 13% for $E_\nu^{CCQE} < 400$ MeV and decreases the background by as much as 20% above this neutrino energy region. Including this correction factor, the uncertainty on the overall NC π^0 backgrounds is 7%. Note that a correction factor of 2.0 would be required to explain the origin of the excess as originating from a misestimated NC π^0 background [Karagiorgi, 2010].

The excess is unlikely caused by a misestimation of the $\Delta \rightarrow N\gamma$ backgrounds because they are additionally constrained by the NC π^0 measurement through the relative rate of resonant production times a branching fraction of (0.56±0.04)%. With this measurement, the uncertainty on the $\Delta \rightarrow N\gamma$ backgrounds is 12%. Note that a (very large) correction factor of 2.7 would be required to explain the origin of the excess as originating from a

misestimated $\Delta \rightarrow N\gamma$ background.

The excess is unlikely caused by a misestimation of the dirt backgrounds because a direct measurement is made by selecting a separate event sample which are likely dirt events and comparing data to simulation. These events are reconstructed close to the detector boundaries with direction pointed generally inwards. In neutrino mode, a dirt background normalization correction factor was computed to be 0.7 ± 0.1 (with simulation over-predicting the dirt rate normalization). Given the power of the event selection cuts designed to mitigate dirt backgrounds, the relevance of this relatively large correction factor is minimal.

The charged current induced backgrounds (intrinsic ν_eCCQE) are reduced with *in situ* measurements of ν_μCCQE interactions. A data to simulation comparison of measured ν_μCCQE interactions allows for the retuning of underlying flux and cross section parameters in order to bring simulated distributions in agreement with data. These parameters are the same as those used to predict the ν_eCCQE rate and shape. In addition, a measurement of the highest energy ν_μCCQE interactions allows for the further constraint of ν_eCCQE from kaon decay backgrounds, which is discussed in more detail in a later section of this thesis.

Given the likelihood that the excess is not caused by misidentified backgrounds, several new-physics interpretations have been proposed in attempt to explain the excess, including sterile neutrino oscillations (with one, two, or more sterile neutrinos), and new interactions both within and outside of the standard model (CPT violation, quantum decoherence, sterile neutrino decay, etc). A summary of these interpretations can be found in [Schwetz, 2008]. A commonality between all interpretations is that their interactions pass the MiniBooNE event selection cuts; that is, they have one electron or one photon exiting the interaction vertex.

5.1.4 MicroBooNE In The Context of the Low Energy Excess

Given the proposed explanations for the origin of the measured MiniBooNE low energy excess in neutrino mode all predict either a single electron or single photon produced at the neutrino interaction vertex, and that MiniBooNE cannot discriminate between single electrons or photons, the MicroBooNE experiment was proposed. This detector (described in detail in Section 3.1) is a liquid argon time projection chamber, a relatively new detector technology which allows for the discrimination between single electrons and photons based on the energy deposition at the start of their tracks (photons will pair produce and in general have twice the ionization as a single electron). MicroBooNE runs in the same beam line (BNB) in neutrino mode and is physically located very close to MiniBooNE. Therefore, MicroBooNE should be able to elucidate the MiniBooNE low energy excess ambiguity.

A preliminary attempt to scale the MiniBooNE backgrounds and excess to MicroBooNE is shown in Figure 5.6, both under the assumption that the excess is due to an electron-like event (left) or due to a photon-like event (right) [UBT, 2012]. The resulting statistical significance after the nominal amount of data is taken in MicroBooNE (6.6×10^20 POT) is computed to be 5.7σ under the single-electron excess hypothesis and 4.1σ under the single-photon hypothesis. Note that this scaling is assuming the electron/photon misidentification rate in MicroBooNE is assumed to be 6% (whereas it is 100% for MiniBooNE). Also event selection efficiencies in MicroBooNE are assumed to be twice that of MiniBooNE because of the detector technology. This scaling procedure ignores other potentially important differences between MicroBooNE and MiniBooNE including differences in detector geometry (important for π^0 misidentifications in which one photon escapes), flux differences (which are non-negligible despite the relative close physical proximity of the two detectors), event topology selection differences (MicroBooNE can see much more vertex activity than can MiniBooNE, especially when additional final state particles are below Cherenkov threshold), the differing cosmic rejection background efficiencies (MiniBooNE can reject cosmics more efficiently than MicroBooNE), cross section differences between argon and CH_2 arising from differing proton to neutron ratios, among other things.

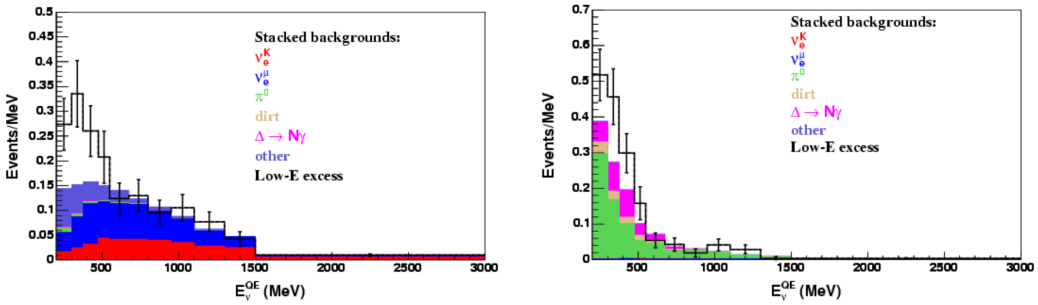

Figure 5.6: *A preliminary attempt to scale the MiniBooNE backgrounds and excess to the MicroBooNE both under the assumption that the excess is due to an electron-like event (left) or under a photon-like event (right). Stacked histograms show the expected background. Error bars indicate statistical uncertainty. The number of signal events, scaled from MiniBooNE for neutrino flux and fiducial volume, is the same in both plots. Both plots assume* 6.6×10^20 *POT for the MicroBooNE 60 ton fiducial mass.*

While the aforementioned scaling of MiniBooNE backgrounds to MicroBooNE provides a reasonable estimate of the expected sensitivity to the MiniBooNE low energy excess, it is oversimplified for the reasons mentioned. The next sections in this thesis describe a more rigorous analysis with the ultimate goal of computing MicroBooNE's sensitivity to the MiniBooNE low energy excess assuming specifically the single-electron hypothesis. In this analysis, signal and background events will be simulated in the MicroBooNE detector and event selection cuts and algorithms will be used to select the events.

5.2 Monte Carlo Simulation

5.2.1 Simulated Background Samples

In this analysis, both beam induced backgrounds and beam external backgrounds are simulated in the MicroBooNE cryostat. For beam-induced samples, the same flux predictions are used as were used in the MiniBooNE simulations (accounting for baseline and acceptance differences). The beam-induced samples come from full simulated BNB interactions with

cross sections provided by GENIE [Andreopoulos *et al.*, 2015][1]. Beam-external samples (cosmics) come from simulated CORSIKA generated [Heck *et al.*, 1998] cosmic rays that pass through the cryostat. Cosmic rays passing through other portions of the detector hall but not the cryostat result in negligible backgrounds in this ν_e search. The passage of all particles through the detector volume is simulated by the GEANT4 package [Agostinelli and others, 2003].

5.2.2 Reconstruction

In general, the output of an automated reconstruction chain in a LArTPC consists of reconstructed optical hits which come from the PMT signals, and reconstructed wire hits which come from drift electron ionization signals on the induction and collection plane wires. Reconstruction algorithms cluster the latter hits on each wire plane into those corresponding tt individual particles, then match clusters from different wire planes to form 3D reconstructed objects. The wire planes provide two of the three dimensions, and matching clusters to optical hits on the PMTs provide the third (drift) dimension. These reconstructed objects are either thin, straight tracks (which come from particles like muons, charged pions, and protons) or more fuzzy showers, which come from higher energy electrons or photons. Ideally this analysis would be done these reconstructed objects. In this way, the same reconstruction methods could be used on data as are used in simulation. While automatic track reconstruction can currently be performed at an adequate level, the difficulties involved in shower reconstruction (which is particularly important to tag and study ν_eCC events) have yet to be overcome.

For these reasons, this simulation-only study is done with objects that are not automatically reconstructed from wire and PMT signals, but instead from truth-based energy depositions in the detector. In general, these objects represent what would be reconstructed

[1]Note that while MicroBooNE uses GENIE to simulate BNB interactions, MiniBooNE used NUANCE [Casper, 2002]. Given the approach to determine the absolute normalization of the MiniBooNE excess as seen in MicroBooNE based on intrinsic nue rates (see Section 5.5), differences between these two generators can be ignored.

from wire and PMT signals if the reconstruction algorithms performed perfectly. Therefore, this is referred to as "perfect reconstruction" and the details of it are discussed in the next section.

5.2.2.1 "Perfect Reconstruction"

While a simulation-only study using real automated reconstruction would be ideal, such a study using "perfect reconstruction" is incredibly valuable; it is a step forward from the aforementioned simple scaling study (Section 5.1.4), and the event selection cuts and algoritihms designed in this study can be used out-of-the-box on automated reconstructed objects once they become available. Additionally, the "perfect reconstruction" can be tuned to more realistically represent what automated reconstruction might be capable of, for example by smearing the energy of objects or emulating realistic reconstruction efficiencies. This will provide the important estimate of uncertainties arising from the imperfect automated reconstruction.

As mentioned earlier, the final 3D reconstructed objects formed from wire plane signals and PMT signals are referred to as tracks or showers. Tracks are close to straight lines in three dimensions, while showers are fuzzier and generally cone-shaped in three dimensions. The "perfect reconstruction" analogs to tracks and showers are referred to as MCTracks and MCShowers. They are created from simulated GEANT4 3D energy depositions in the detector volume. GEANT4 outputs 3D energy depositions in the detector, along with truth information about which parent particles deposited this energy. MCShowers and MCTracks are 3D objects which are formed by grouping energy depositions based on parent particles. Whether a particle in GEANT4 becomes an MCShower or an MCTrack is based on truth PDG (for example, electrons always form MCShowers[2] and muons always form MCTracks). Only the energy deposited by particles *within the TPC* is used to form these "perfect reconstructed" objects, which is in line with them representing actual reconstructable quantities (no ionization outside of the TPC is reconstructable).

[2]Despite the fact that electrons behave more like tracks below the critical energy, which is on the order of 40 MeV in liquid argon

To clarify, consider the following simulated interaction: a ν_e charged current interaction in which the final state particles are an electron, a charged pion, a neutral pion, and two protons. The charged pion travels until it stops, where it decays into a muon, which then travels and decays into an electron. The generated "perfect reconstruction" objects in the event will be four MCShowers (for the electron exiting the interaction, the electron from the muon decay, and one for each photon originating from the neutral pion decay) and four MCTracks (one for the charged pion, one for the muon, and one for each proton).

MCTracks consist of a series of ordered 3D trajectory points, each corresponding to an energy deposition in the detector. MCShowers have the following attributes: 3D start point where the first energy from the parent particle is deposited, 3D direction which is computed by fitting a line in 3D to all of the deposited energy from the parent particle, and dE/dx computed from the energy depositions along the first few centimeters of the shower. These "perfectly reconstructed" tracks and showers (MCTracks and MCShowers) serve as the input to the event selection algorithms, just as automated reconstructed tracks and showers (with the same attributes) would in real data.

5.3 Event Selection

This section describes the algorithms and cuts used to identify ν_e^{CC} interactions, given as input the "perfect reconstructed" MCTracks and MCShowers from simulated triggered events in MicroBooNE[3]. With these reconstructed objects in hand, a series of nine algorithms are run, each with a specific goal in mind; they either identify background topologies in order to remove them, or they identify the signal ν_e^{CC} topology. For example, one algorithm identifies MCShowers which are likely delta rays originating from tracks. Once identified, these MCShowers are no longer candidate ν_e^{CCQE} electrons. Another algorithm

[3]Note that these cuts and algorithms could use automatically reconstructed tracks and showers, and therefore could be run both on simulation and data, if the quality of track and shower reconstruction was high enough.

looks for pairs of showers that are likely from π^0 decays (by using the dE/dx of those showers, and requiring they back-project to a common origin) in order to remove them from the pool of candidate ν_e^{CC} electrons. Another algorithm looks for through-going tracks to tag them as cosmic, ensuring they will not be associated with a neutrino interaction. The two most important event selection algorithms for this analysis are named "AlgoEMPart" (which handles the electron/photon discrimination based on MCShower deposited energy near its start point) and "AlgoSingleE" (which is the algorithm responsible for locating the ν_e^{CC} topology and associating all MCTracks and MCShowers together for eventual energy reconstruction and analysis). These two algorithms are discussed in detail in the following two subsections. The remaining seven event reconstruction algorithms are discussed in detail in the appendices of this thesis. Note that at the end of the chain of event selection algorithms, a sample of candidate ν_e^{CC} events is tagged. These events are the subject to further cuts both to mitigate some backgrounds that the event selection algorithms missed, and more importantly to pick specifically ν_e^{CCQE} events so as to make the eventual comparison to the MiniBooNE excess, since MiniBooNE searched for ν_e^{CCQE} events, not ν_e^{CC}.

5.3.1 Electron/Photon Separation Algorithm

Electron/photon separation based on dE/dx at the start of showers is done through an algorithm called "AlgoEMPart". This algorithm uses trained likelihood distributions which input dE/dx and return the likelihood that the shower is electron-like, or photon-like. If a conversion distance (the distance between the reconstructed start point of the shower and the first energy deposition of the shower) is known, it will incorporate that into its likelihood as well. The likelihood is configured with parameters output by a RooFit [Verkerke and Kirkby, 2003] minimization routine. The RooFit routine is trained on simulated single electron and single photon MCShowers. In general, this algorithm computes both the likelihood that an MCShower is an electron and that it is a photon, and determines the identity of the particle to be the one with the larger likelihood.

There are two likelihood functions that may be used. If an MCShower can indepen-

dently be associated with a neutrino interaction vertex, AlgoEMPart will use a 2D likelihood function that includes both dE/dx and radiation length information. If an algorithm cannot associate a vertex with a shower, there is a 1D likelihood function that can be used with only dE/dx information. The 1D likelihood function is composed of a gaussian plus a landau distribution for dE/dx, and the 2D likelihood function also includes an exponential function for radiation length. Any potential energy dependence on dE/dx or conversion distance is not included in these likelihoods. The twelve trained input parameters include mean and sigma values for the gaussian distributions, the MPV and sigma values for the landau distributions, the fractional area difference between the gaussian and landau distributions, and the radiation length parameter (six parameters for electrons, six parameters for photons). When training, input parameters for each sample (electron, photon) are the MCShower computed dE/dx as well as the truth-level creation vertex of the particle. The training results on "perfect reconstruction" electron and photon showers are shown in Figures 5.7, then zoomed in in Figure 5.8.

5.3.1.1 Performance

The performance of this algorithm on "perfect reconstruction" is computed by using samples of single electron showers and single photon showers generated isotropically between 0.05 and 2 GeV, and selecting those events where greater than 90% of the shower's energy is contained within the TPC. The algorithm's likelihood is trained using this sample (integrated over the full energy range of the showers). The efficiency to tag electrons and photons both with the 1D and the 2D likelihood are enumerated below.

1. Using *only dE/dx* information, the efficiency (over all energies) to select a single electron is 93%, while the MID efficiency to tag the electron as a photon is 7%.

2. Using *only dE/dx* information, the efficiency to select a single photon is 97.3%, while the MID efficiency to tag the photon as an electron is 2.7%.

3. Using *both dE/dx and radiation length* information (using the true creation point of photons), the efficiency to select a single electron is 99.7%, while the MID efficiency to tag the electron as a photon is 0.3%.

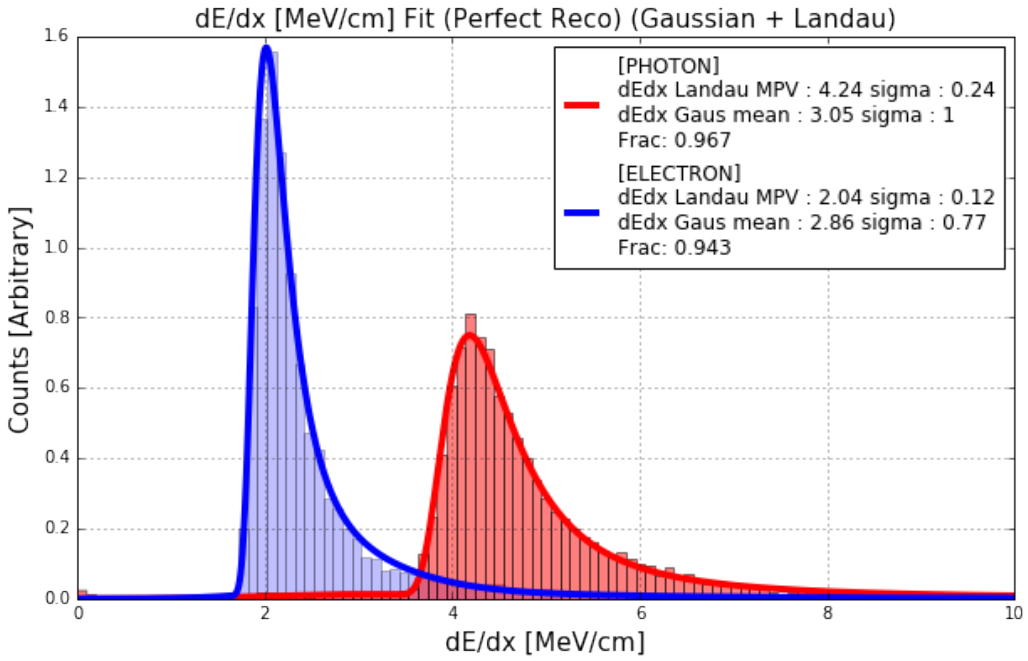

Figure 5.7: *AlgoEMPart training results on perfect reconstructed electron showers and on perfect reconstructed photon showers as described in Section 5.3.1.1: 1D landau + gaussian fit to dE/dx.*

4. Using *both dE/dx and radiation length* information (using the true creation point of photons), the efficiency to select a single photon is 98.1%, while the MID efficiency to tag the photon as an electron is 1.9%.

The 1D likelihood to determine if a shower is electron-like or photon-like is shown in Figure 5.9. The likelihood that a shower with a given dE/dx is electron-like is computed by the ratio of the 1D electron-like probability distribution function (PDF) value for that dE/dx (shown non-normalized in Figure 5.7) to the sum of the electron-like PDF value for that dE/dx and the photon-like PDF value for that dE/dx (shown non-normalized in Figure 5.7 as well) (Equation 5.2).

$$LL_e = \frac{e^{PDF}_{dE/dx}(\frac{dE}{dx})}{e^{PDF}_{dE/dx}(\frac{dE}{dx}) + g^{PDF}_{dE/dx}(\frac{dE}{dx})} \tag{5.2}$$

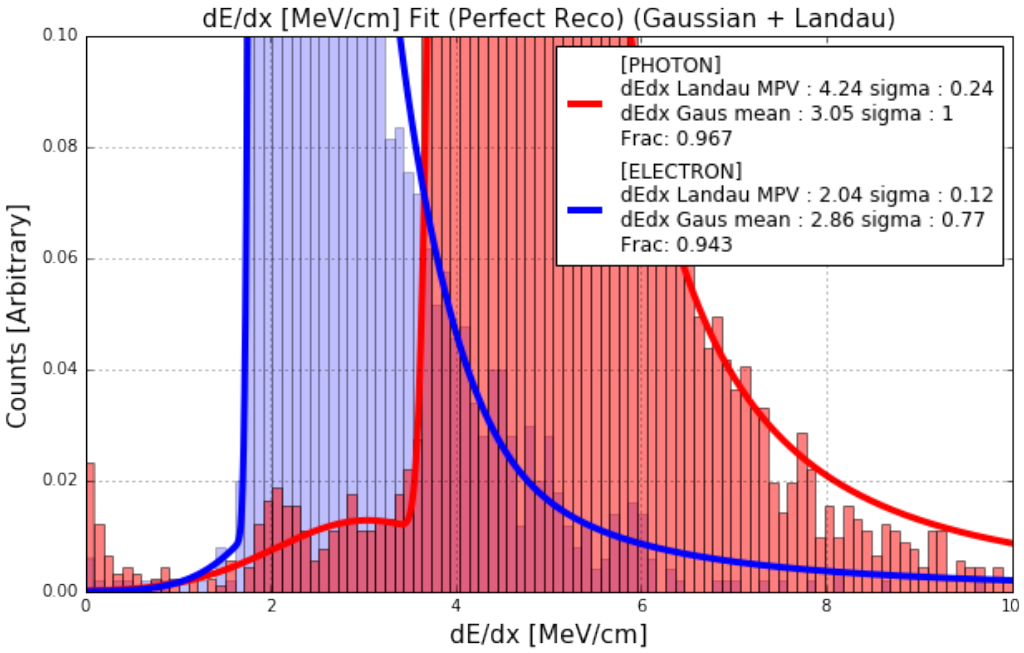

Figure 5.8: *The same plot as shown in Figure 5.7, but zoomed in along the y-axis to show the compton peak in the photon sample, as well as the pileup of very low dE/dx values for photons (due to soft compton scatters as described in Section 5.2.2.1).*

where $e^{PDF}_{dE/dx}(\frac{dE}{dx})$ represents the electron dE/dx PDF function (shown non-normalized in Figure 5.7) evaluated at a dE/dx value $\frac{dE}{dx}$ and $g^{PDF}_{dE/dx}(\frac{dE}{dx})$ represents the photon dE/dx PDF function (also shown non-normalized in Figure 5.7) evaluated at a dE/dx value $\frac{dE}{dx}$. The likelihood that a shower with a given dE/dx is photon-like is similarly computed but with the photon-like PDF value for that dE/dx in the numerator.

The 2D likelihood including both dE/dx and conversion distance is shown in Figure 5.13. The likelihood that a shower with a given dE/dx value, $\frac{dE}{dx}$ and a given conversion distance value, d is electron-like is computed as follows:

$$LL_e = log(\frac{e^{PDF}_{dE/dx}(\frac{dE}{dx}) * e^{PDF}_{conv}(d)}{g^{PDF}_{dE/dx}(\frac{dE}{dx}) * g^{PDF}_{conv}(d)}) \tag{5.3}$$

where $e^{PDF}_{dE/dx}(\frac{dE}{dx})$ represents the electron dE/dx PDF function (shown non-normalized in Figure 5.7) evaluated at a dE/dx value, $\frac{dE}{dx}$, $e^{PDF}_{conv}(d)$ represents the electron conversion

distance PDF function (shown non-normalized in Figure 5.10) evaluated at a conversion distance value, d, $g^{PDF}_{dE/dx}(\frac{dE}{dx})$ represents the photon dE/dx PDF function (shown non-normalized in Figure 5.8) evaluated at a dE/dx value, $\frac{dE}{dx}$, $g^{PDF}_{conv}(d)$ represents the photon conversion distance PDF function (shown non-normalized in Figure 5.11) evaluated at a conversion distance value, d. The likelihood that the same shower is photon-like is simply the inverse of Equation 5.3.

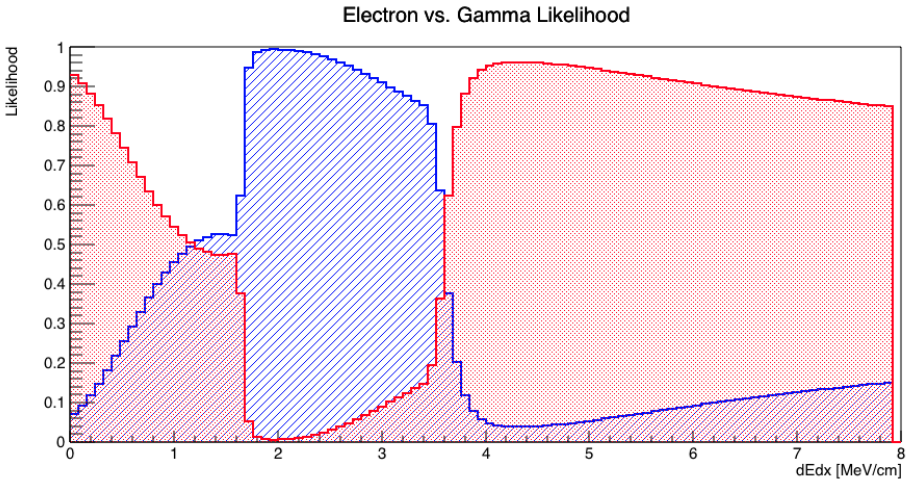

Figure 5.9: *AlgoEMPart: Computed 1D likelihood vs dE/dx: red is photon, blue is electron. How the likelihood is computed is described in Section 5.3.1.1.*

5.3.2 Signal Selection Algorithm

The purpose of this algorithm is to reconstruct events with ν_eCC inclusive type topologies. These topologies involve a single electron at a neutrino interaction vertex, with any number of protons, charged or neutral pions, or anything else additionally exiting the vertex. Later on, the sample of selected events will be subjected to further cuts to select only ν_eCCQE topologies by rejecting events with pions in the final state. This algorithm uses likelihoods provided by AlgoEMPart (Section 5.3.1) to determine if a shower is an electron or a photon. This algorithm begins by looping over all candidate ν_eCC electron showers in the event that have not been removed by upstream cosmic and π^0 tagging algorithms. Figure 5.14 is a

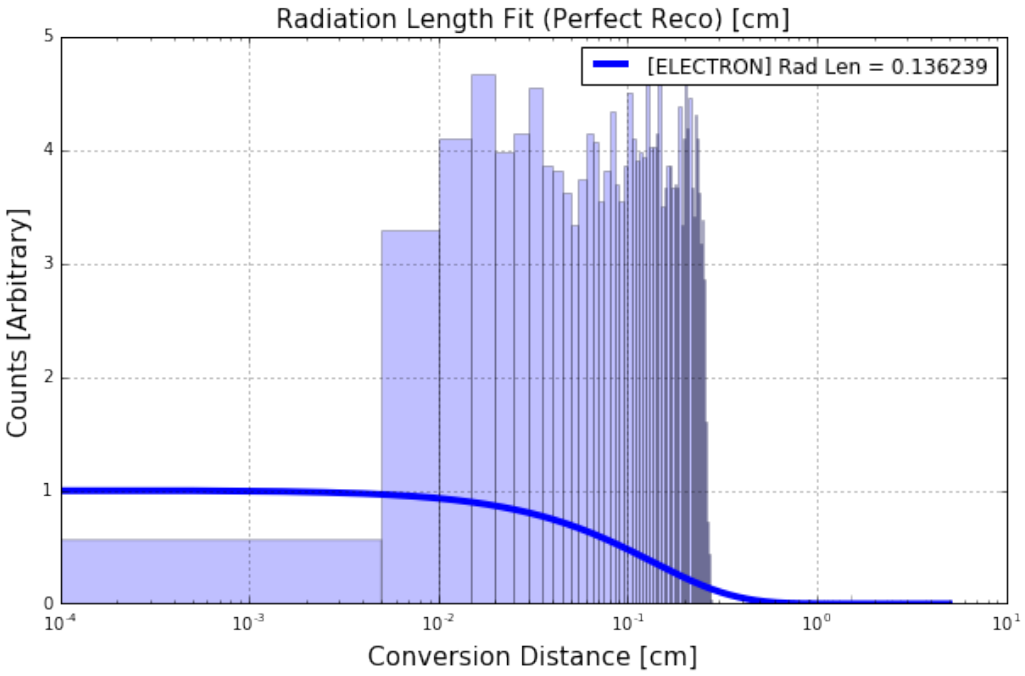

Figure 5.10: *AlgoEMPart training results on perfect reconstructed electron showers as described in Section 5.3.1.1: Radiation length fit to single electron showers. Note the poor quality of the fit as the electron conversion distance for "perfect reconstruction" does not follow an exponential distribution; all conversion distances are below 0.3 centimeters.*

flowchart depicting decisions the algortihm makes for each candidate ν_eCC electron shower. If the algorithm reaches the bottom of the flowchart, that shower is determined to be from a ν_eCC interaction and the event is saved to be included in analysis. The flowchart refers to determining if two showers are correlated and determining if a shower is correlated with the start of a track. A schematic which diagrams how these determinations are made is shown in Figure 5.15. A list of configurable parameters and their chosen cut values can be found in Table 5.1. A more detailed description of Figure 5.14 is given in the following paragraphs.

For each primary, non-cosmic shower ("shower A"), this algorithm computes the point of closest approach and impact parameter between the shower's back-projection and to all other tracks, as well as to all other shower back-projections (see Figure 5.15). If the smallest impact parameter (IP) is less than 10 centimeters and the distance between the shower's

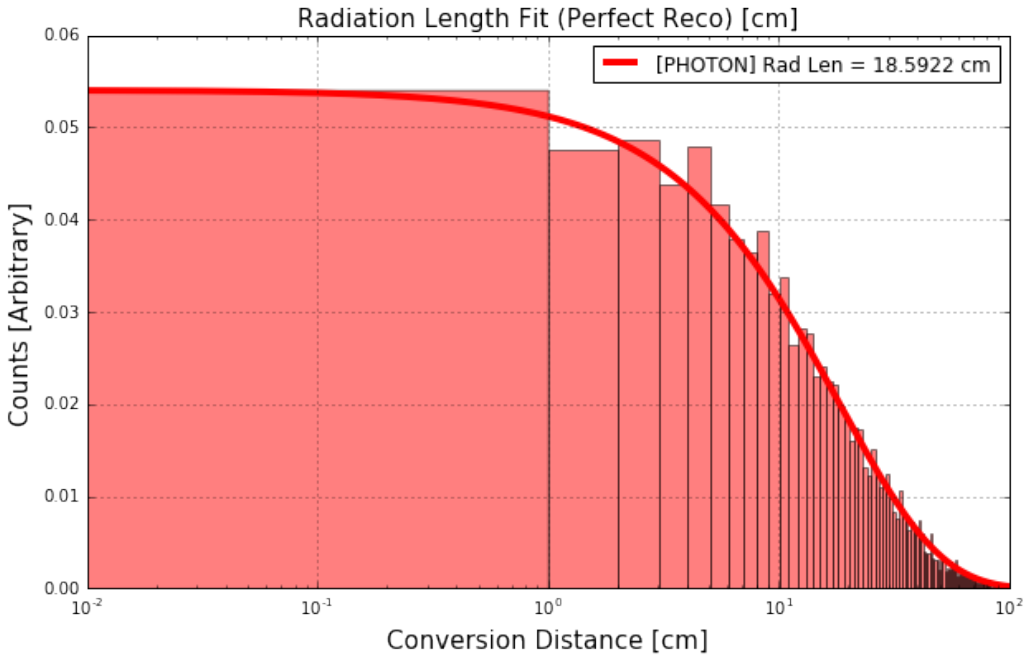

Figure 5.11: *AlgoEMPart training results on perfect reconstructed photon showers as described in Section 5.3.1.1: Radiation length fit to single photon showers.*

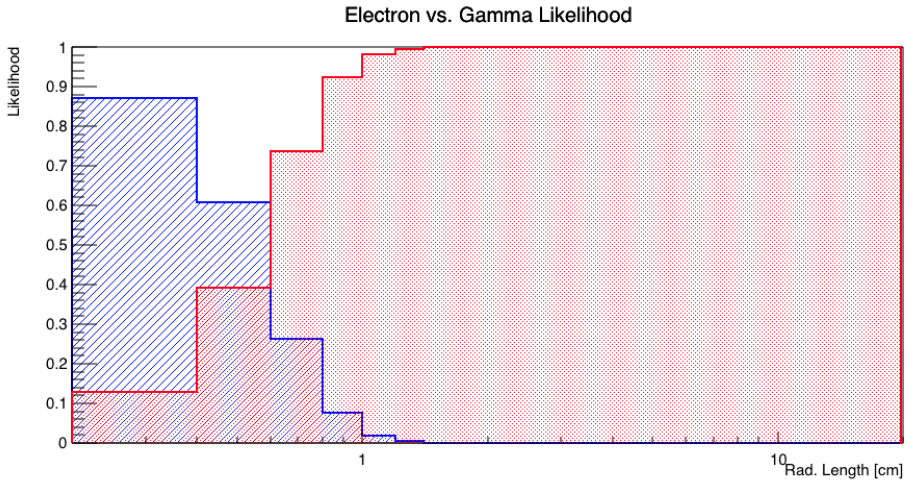

Figure 5.12: *AlgoEMPart: Computed 1D likelihood vs conversion distance (integrated over all energies): red is photon, blue is electron. How the likelihood is computed is described in Section 5.3.1.1.*

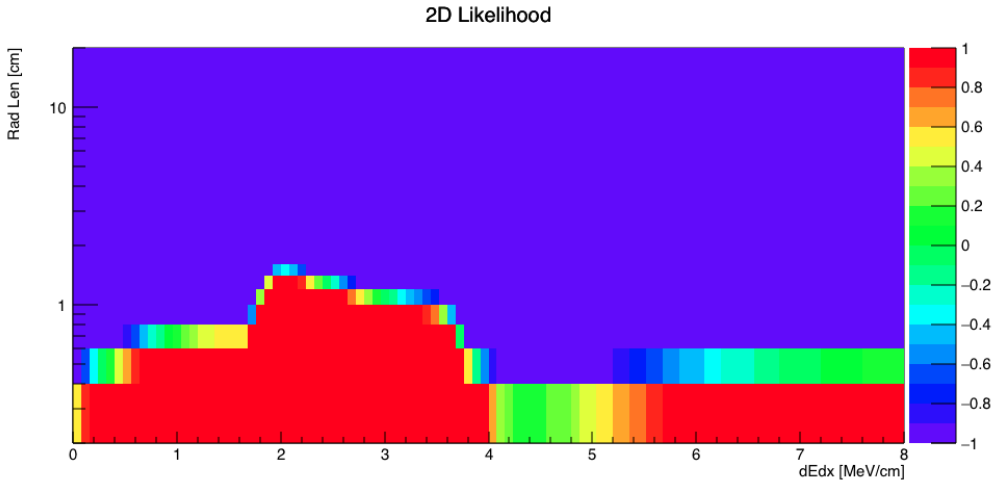

Figure 5.13: *AlgoEMPart training results on perfect reconstructed electron and photon showers as described in Section 5.3.1.1 integrated over all energies: 2D likelihood distribution (radiation length vs. dE/dx). Low values of likelihood (purple) correspond to photon-like, high values (red) correspond to electron-like.*

start point and the point of closest approach (Vertex-to-Shower-Start-Distance) is greater than 1 centimeter, the algorithm assumes this shower is a photon and it rejects the shower as a potential ν_eCC shower, without any dE/dx considerations[4]. Otherwise, the algorithm continues by using AlgoEMPart's trained likelihood function to determine based on dE/dx alone whether this shower is gammalike and should therefore be ignored.

Assuming this potential ν_eCC shower ("shower A" in Figure 5.15) has so far been found to be electron-like, the algorithm then compares the shower to all other showers in the event that are not marked as cosmic, and are not already reconstructed to be the descendant of another particle. The purpose of this portion of the code is to enforce that the topology of interest includes a *single electron* exiting the neutrino interaction. If any other electron-like showers are nearby (with Vertex-To-Shower-Start-Distance less than _vtxToShrStartDist

[4]Note that for ν_e^{CC} interactions and "perfect reconstruction", these impact parameters and points of closest approach between the ν_e^{CC} electron shower and other tracks in the event are incredibly small (sub centimeter). The cut values are chosen to be much larger to simulate estimated automatic track and shower reconstruction resolutions.

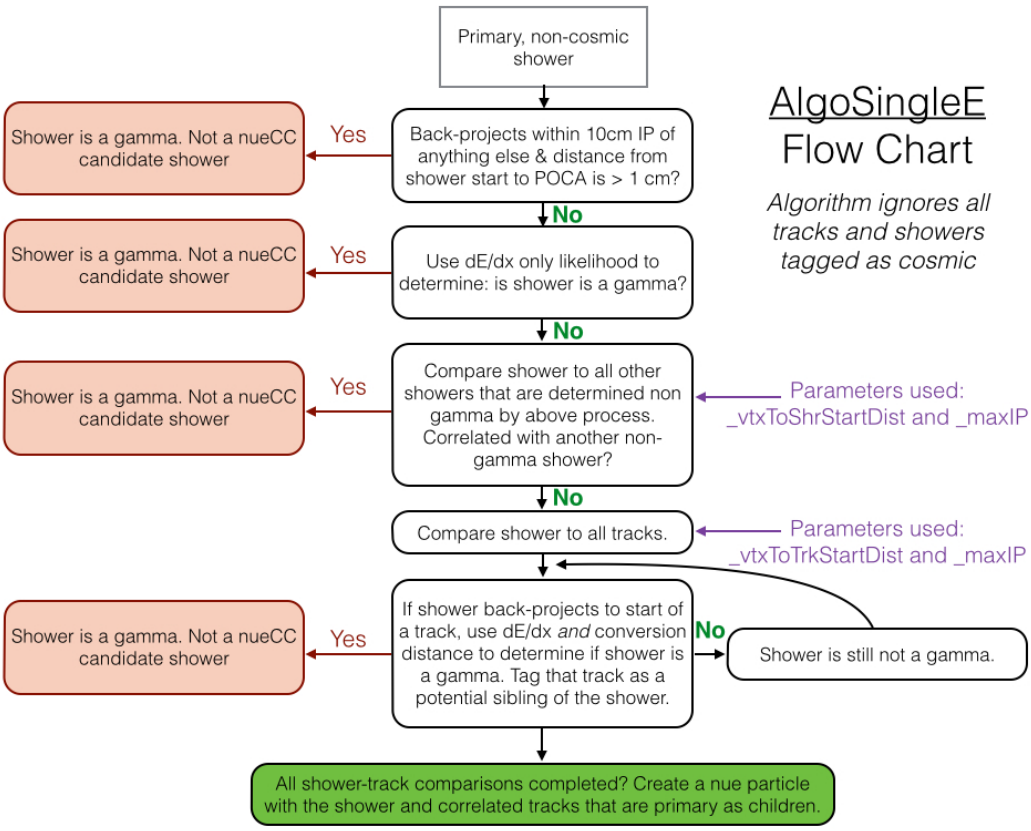

Figure 5.14: *A flowchart depicting decisions the algortihm makes for each primary, non-cosmic shower. If the algorithm gets to the bottom of the flowchart, that shower was determined to be from a ν_eCC interaction, and a ν_e particle is created.*

and IP less than _maxIP) that could be potentially correlated, "shower A" is rejected as a candidate ν_eCC electron.

Assuming "shower A" has not yet been rejected, it is then compared to every track in the event that has not been tagged as cosmic and is longer than 0.3cm (a value chosen because it is the wire spacing and tracks shorter than one wire spacing are assumed non reconstructable). The purpose of this portion of the code is to look for correlations between the potential ν_eCC electron and tracks (Figure 5.15). The topology of interest allows for the electron to point back to the *start* of a track, but *not* to the middle or end of a track (as these showers are likely delta rays or Michel electrons). For each "shower A"-to-track com-

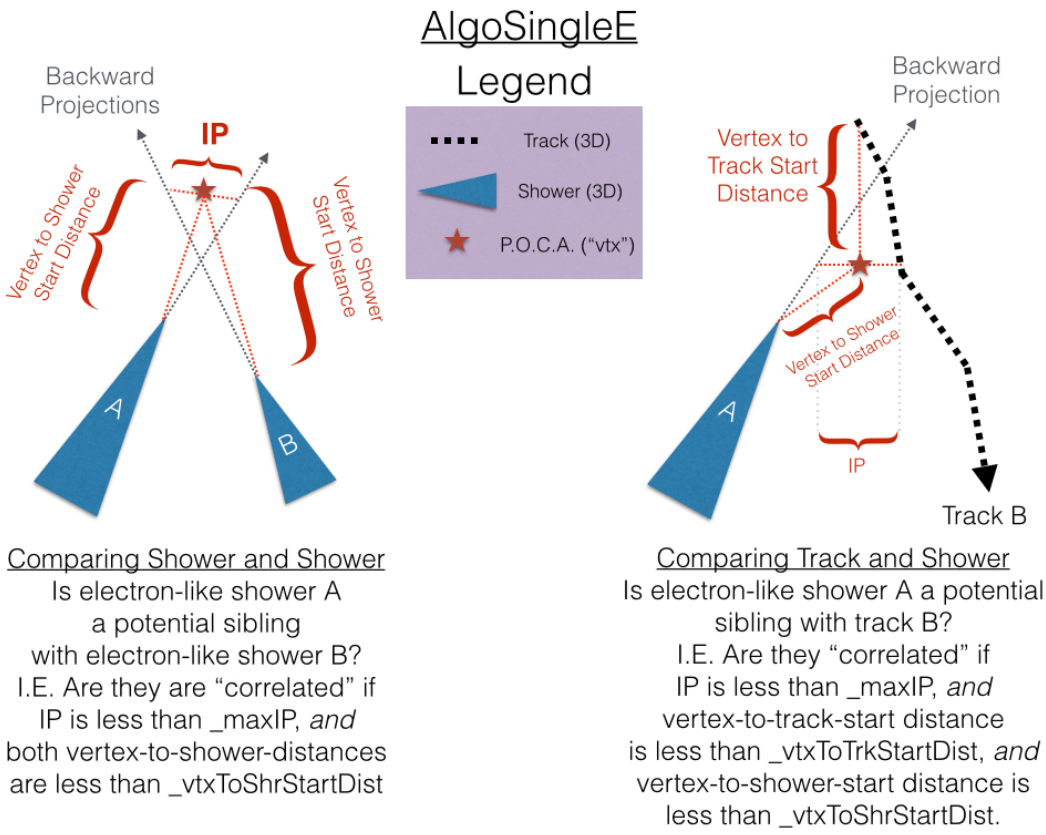

Figure 5.15: *Schematic cartoons indicating how the signal selection algorithm makes decisions determining if two reconstructed showers are correlated, and if a reconstructed shower is correlated with a reconstructed track (as described in Figure 5.14).*

parison, the point of closest approach (P.O.C.A.) between the shower's backward projection and the track's trajectory is computed. If the impact parameter between the shower and the track is less than a configurable distance (_maxIP) and the distance between the start point of the track and the P.O.C.A. is less than a configurable distance (_vtxToTrkStartDist) and the distance between the start point of the shower and the P.O.C.A. is less than a configurable distance (_vtxToShrStartDist) then there is a potential acceptable correlation between "shower A" and the start of the track. At this point, the code again uses a likelihood from AlgoEMPart to determine if the shower is still electron-like, this time using both the shower's dE/dx *and* the distance between the shower start and the computed P.O.C.A. as a radiation length. This is a more powerful discrimination to determine if the shower

AlgoSingleE: Parameters		
Parameter Name	Code Variable	Cut Value
Use Radiation Length	_useRadLength	True
Max Vertex-to-Track-Start Distance	_vtxToTrkStartDist	1 cm
Min Vertex-to-Shower-Start Distance	_vtxToShrStartDist	50 cm
Maximum IP	_maxIP	1 cm

Table 5.1: *The list of configurable parameters and their values used in the AlgoSingleE ν_e^{CC} signal selection algorithm. Note that for ν_e^{CC} interactions and "perfect reconstruction", these actual values the distance-based parameters represent are incredibly small (sub centimeter). The cut values are chosen to be much larger to simulate estimated automatic track and shower reconstruction resolutions.*

remains electron-like. If "shower A" remains electron-like and is found to be correlated with the start of a track, the track is stored as associated with another final state particle of the ν_e^{CC} interaction.

If "shower A" has not yet been rejected, a ν_eCC event has been found, and the event is stored to be included in the analysis.

5.3.2.1 Configurable Parameters

The configurable parameters for this algorithm are summarized in the Table 5.1. Note that with "perfect reconstructed" showers, these distances are always very small (less than 0.1 centimeters), so these values were chosen to introduce some realism into the algorithm by estimating detector resolutions.

5.3.3 Energy Reconstruction

With the candidate ν_eCC interactions identified, the neutrino energy is reconstructed in two ways. First, the angle and energy of the selected ν_eCC electron is used to compute an energy, E_ν^{CCQE} from the CCQE formula, Equation 5.1. This is the same energy definition that is used in the MiniBooNE oscillation analysis. Note that this energy is only valid for truly ν_e^{CCQE} interactions, which are a subset of the selected ν_e^{CC} sample.

An additional, more accurate energy estimation, E_{calo} is calculated by looping over all particles tagged as descendants of the reconstructed ν_e and adding up their deposited energies. For ν_eCC events, this amounts to adding the deposited energy of the electron shower, along with the deposited energies from all protons exiting the interaction vertex, and energies from neutral pions exiting the vertex (adding the pion masses). Additionally the electron mass is added, though this changes the calculated energy negligibly. Plots describing the neutrino reconstruction performance for correctly identified ν_eCCQE interactions can be seen in Figures 5.16 and 5.17. The energy resolution for true neutrino energies below 500 MeV is on the order of 15%, and the bias indicates that the energy reconstruction method tends to underestimate true neutrino energy by about 25%. Note that this bias is computed as the standard deviation of all events in a specific true energy bin rather than the width of a gaussian fit to the central distribution of events, so the bias is skewed down by outliers.

5.4 Backgrounds

5.4.1 Background Topologies

5.4.1.1 Intrinsic ν_e

The intrinsic ν_e^{CCQE} background comes from ν_e^{CCQE} interactions from Booster Neutrino Beam (BNB) electron neutrinos. The topology of these events involve one electron in the final state, with any number of protons exiting the interaction vertex, but no pions or muons exiting the interaction vertex. Neutral particles included in hadronic activity are

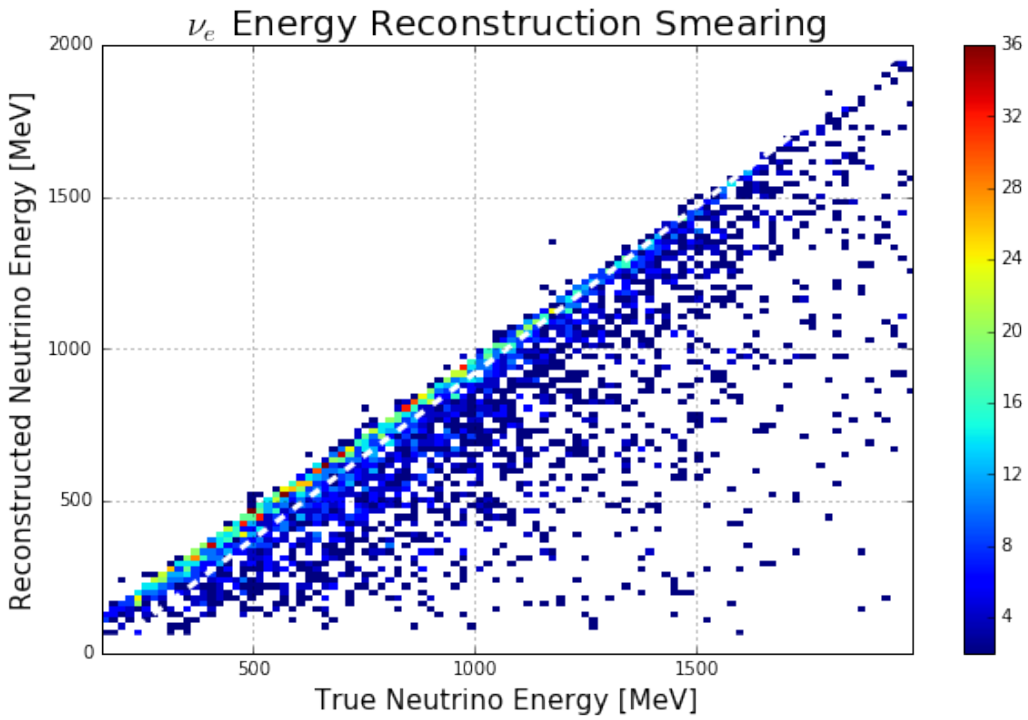

Figure 5.16: *Reconstructed neutrino energy as described in Section 5.3.3 versus true neutrino energy. This plot was made from "perfect reconstruction" objects in correctly identified ν_eCCQE events after all final analysis cuts were placed.*

also ignored as they are invisible from the point of view of a LArTPC. This background is irreducible for a ν_e^{CCQE} appearance search, and the dominiant background in this analysis. These intrinsic ν_es in the relevant low energy region are mostly from muon decay in the beam line. The flux uncertainty can be constrained by a parallel ν_μ analysis, as was done in MiniBooNE. While constraining ν_e from muon decay in the beam line with a parallel ν_μ analysis, constraining ν_e from kaon decay in the beam line is discussed in the next chapter of this thesis.

5.4.1.2 Intrinsic ν_μ

The intrinsic ν_μ background comes from ν_μCC interactions from BNB muon neutrinos. Despite the enormous ratio of ν_μCC events to ν_eCC events, this is a subdominant background in this analysis. Potential sources of misidentifications (MIDs) must always involve at least

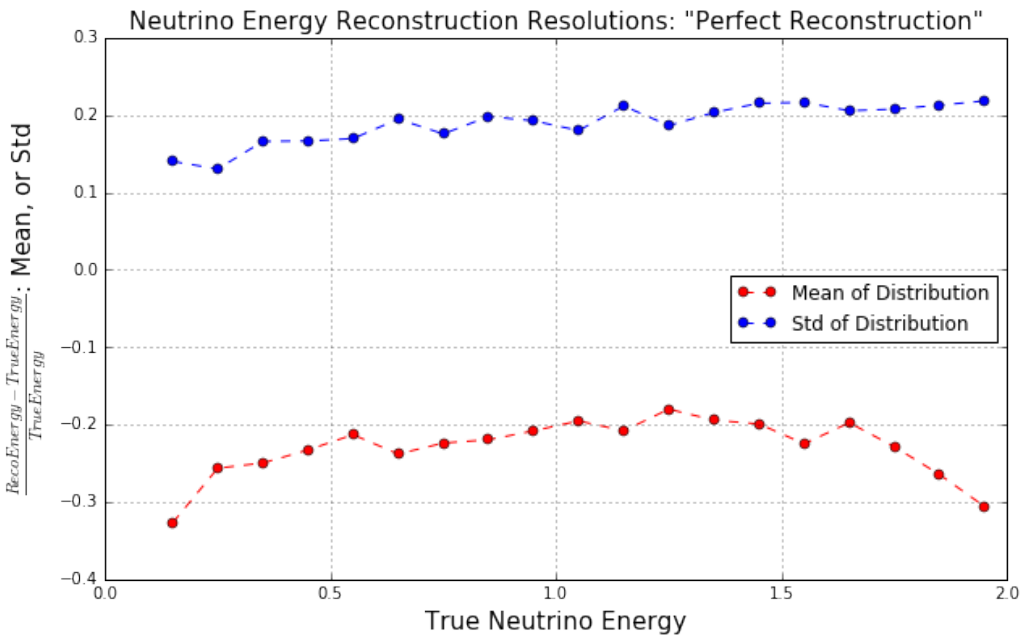

Figure 5.17: *A neutrino energy resolution and bias plot. This is created by binning Figure 5.16 in true neutrino energy and making a distribution of (Reco Energy - True Energy)/(True Energy). For each bin, the mean (red) and standard deviation (blue) are plotted in the above figure. This plot was made from "perfect reconstruction" objects in correctly identified ν_eCCQE events after all final analysis cuts were placed.*

one shower. For this reason, most ν_μCC MIDs are from either

1. μ decay electrons (either in flight, or at rest when the energy of the electron is in the very high end of the Michel spectrum), or

2. ν_μCC events with a neutral pion in the final state.

The first source is suppressed because the electron points back to the end of the muon track and therefore is generally tagged by event selection algorithms. However, this background may be more prominent if the muon reconstructed track direction gets flipped (after which, the electron would point back to the *start* of the muon track). The effect of flipping this track is not included in this analysis, but the impact is expected to be small because there are several handles on track directionality in LArTPCs including from multiple Coulomb scattering and delta rays. The second source occurs when one of the photons of the neutral

pion decay from a $\nu_\mu^{CC}\pi^0$ interaction is misidentified as an electron. This background is greatly suppressed because the dE/dx of the shower should be photon-like, and the shower points back towards the muon start point. The fact that the shower is displaced from the muon start point allows for a photon-like likelihood calculation using both the shower dE/dx and the radiation length, which is a more powerful discrimination tool to tag the shower as being from a photon (as decribed in Section 5.3.1). Additionally, if the second photon converts inside of the detector, this provides another handle that the shower is from a neutral pion.

5.4.1.3 Intrinsic Neutral Current (NC)

The intrinsic NC background comes from neutral current interactions by any neutrino type from the beam. In these interactions, the neutrino interacts with the exchange of a neutral Z boson, and the neutrino carries off some energy and momentum as it exits the detector. This fact (that the summed momenta of all children from the interaction won't point along the beam direction) can be leveraged to mitigate these backgrounds. The predominant NC background for the low energy excess analysis are ν_x (mostly ν_μ) interactions with a neutral pion in the final state. This was by far the most dominant background in the MiniBooNE ν_e appearance analysis. In this topology, one of the photons from the neutral pion decay is mis identified as an electron coming from a ν_eCC interaction. This background is significantly mitigated when both photons convert inside of the detector. In that case, the presence of two showers pointing back to a common origin allows for the event to be rejected.

An additional NC background topology is NC $\Delta \rightarrow N\gamma$, though this background is subdominant to the aforementioned neutral pion decays.

5.4.1.4 Beam-Induced, TPC External ("B.I.T.E.")

This background comes from beam neutrino interactions that occur outside of the TPC volume, but inside of the cryostat volume (including the cryostat walls). By volume (and mass), this region is roughly half of the volume of the entire cryostat. The predominant topology for this background are neutrino interactions involving a neutral pion in the final

state where only one photon from the pion decay converts inside of the TPC. Since this photon may not point back to any other reconstructed objects in the TPC, only its dE/dx can be used in the electron/photon separation likelihood which provides less descrimination power than if a radiation length could be used as well. Note that this analysis does not explicitly ask for a visible hadronic vertex, otherwise many of these backgrounds would be mitigated (though much of the signal would be mitigated as well). In this analysis, this background can be mitigated with cuts like backward-projected distance to a TPC wall, since they are all coming from outside of the TPC.

5.4.1.5 Cosmic

This background comes from cosmic rays that pass through the detector. The relatively high cosmic rate inside of the detector hall makes for on the order of tens of cosmic rays passing through the detector during the full readout window. MID topologies include but are not limited to showers that radiate off of cosmic ray muons, and showers born from cosmic neutron scatters. The vast majority of MIDs from cosmics can be removed by requiring the reconstructed neutrino interaction is matched to a flash inside of the beam gate window. Given the ratio of beam gate window size to readout window size ($\frac{1.6\mu s}{4.8ms} = 0.0003$), this requirement mitigates almost all of the cosmic backgrounds. However, the majority of triggered beam events are not triggered by a neutrino interaction in them but are instead triggered by cosmics that arrived during the beam gate window. These events are referred to as "in-time" cosmics. Given the number of readouts triggered by cosmics inside of the beam gate window rather than neutrinos arriving inside of the beam gate window, the cosmics background can be sizeable, especially in the relevant low energy region. It should be noted that a proper handling of these "in-time" cosmics will take into account events in which a cosmic flash inside of the beam gate window triggers a readout, and a reconstructed ν_e MID associated with a *different* cosmic in the event gets incorrectly matched to the flash inside of the beam gate window.

In addition to these "in-time" cosmics (those that triggered a readout and arrived during the beam gate window), an additional cosmic background comes from events in which

a *neutrino* interacts inside of the beam gate window, triggering a readout, but an out-of-time cosmic MID gets incorrectly matched to the neutrino flash. These cosmic MIDs are appropriately referred to as "out-of-time" cosmics. The "out-of-time" cosmic background is not included in this analysis, but its size relative to the "in-time" cosmics is small.

5.4.2 Background Normalization

As described in Section 5.2.1, the simulated background samples used in this analysis can be classified either as beam-induced, or cosmic. Each beam-induced background has an associated simulated POT generated, and they are each normalized to 6.6×10^{20} POT, the nominal amount of beam scheduled to be delivered to MicroBooNE over the course of three years running. The cosmic simulated sample does not have an associated POT, but instead has an associated total exposure time. The normalization of this sample must involve disregarding the event selection cut in which a reconstructed optical flash occurs within the timing of the beam gate window. The total beam-gate-open exposure time corresponding to 6.6×10^{20} POT is 211 seconds. Therefore, a simple scale factor can be computed based on the simulated cosmic exposure time. Note that treatment of the cosmic background in this way is assuming that the reconstructed neutrino interaction in the TPC has been correctly flash-matched.

5.4.3 Analysis Cuts and Results

A number of additional analysis cuts are placed on the selected candidate ν_eCC events. The purpose of these cuts is to first downsample the selected ν_eCC selected events into a sample of ν_eCCQE events by removing those reconstructed as having pions in the final state. An additional reason to place these cuts is to mitigate backgrounds that the event selection algorithms were unable to remove themselves. The analysis cuts used are described here.

The analysis cuts placed are:

1. The reconstructed ν_e interaction is matched to a flash inside of the beam gate window (this cut is not placed on the cosmic background simulated sample for reasons

described in Section 5.4.2).

2. If the reconstructed ν_e interaction has additional particles reconstructed to be in the final state, those particles are limited to protons only (using assumed perfect efficiency to tag a track as a proton). This downsamples the ν_e^{CC} selected sample to specificially ν_e^{CCQE}.

3. Minimum primary ν_eCC reconstructed electron energy deposited of 60 MeV.

4. A fiducial volume of 10cm from all sides of the detector is placed on the neutrino interaction vertex.

5. A projected-backwards-distance-to-wall cut of 40 cm is placed on the primary ν_eCC reconstructed electron.

The projected-backwards-distance-to-wall cut is computed by back-projecting the reconstructed ν_eCC electron along its shower axis until it intersects with the TPC boundaries. The distance between the electron start point and the wall intersection point is the distance on which the cut is placed.

The efficiency of the event selection algorithms with "perfect reconstruction" inputs to select signal events and to select background events ("MID efficiency") is summarized in Table 5.2. The numerator of this efficiency is the number of events tagged as ν_eCCQE candidate interactions and the denominator is the true number of events with the specified interaction type. The second column in the table does not include the additional final analysis selection cuts which are placed on the reconstruction interactions in the efficiency numerator, and the third column does. The background categories are described in more detail in Section 5.4.1. In the case of the cosmic background category, the denominator is the true number of events triggered by a cosmic arriving within the beam gate window that do not include a neutrino interaction.

The backgrounds to the ν_eCCQE appearance search in MicroBooNE are shown in Figure 5.18, normalized to the nominal MicroBooNE expected POT. The event selection is

Event Selection Efficiencies		
True Event Type	Efficiency	Efficiency Including Analysis Cuts
ν_eCCQE	0.8209	0.6142
ν_μCC	0.0068	0.0002
ν_xNC	0.0086	0.0013
B.I.T.E.	0.0107	0.0005
Cosmic	0.0588	0.0012

Table 5.2: *Event selection efficiencies on "perfect reconstruction".*

described in Section 5.3, the background topologies described in Section 5.4.1, the relative normalization between samples described in Section 5.4.2, and the energy reconstruction described in Section 5.3.3.

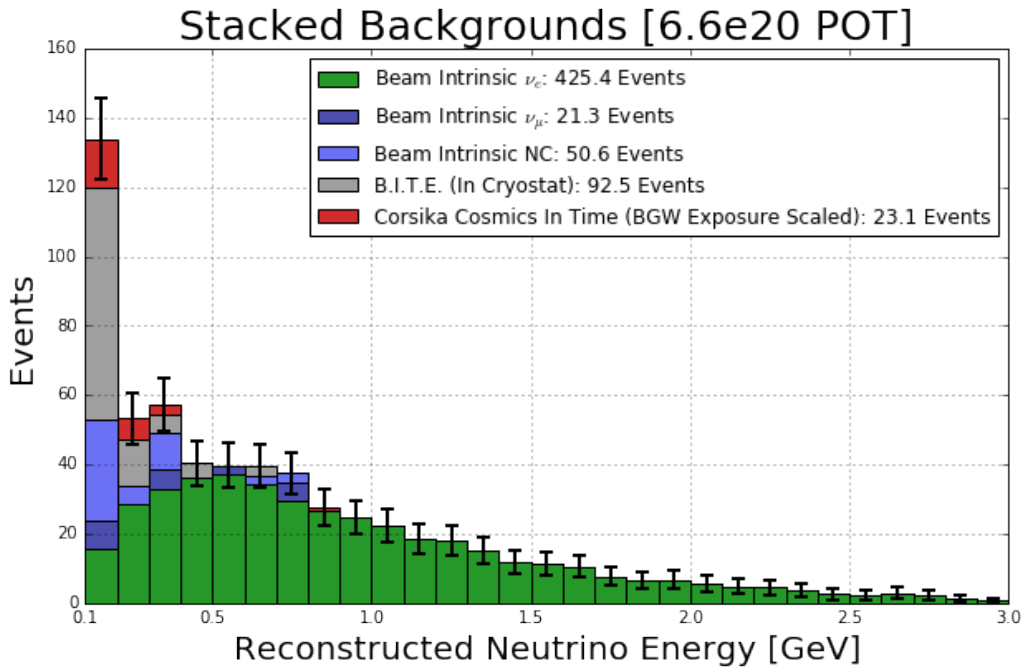

Figure 5.18: *The backgrounds to the ν_eCCQE appearance search in MicroBooNE. The event selection is described in Section 5.3, the background topologies described in Section 5.4.1, the relative normalization between samples described in Section 5.4.2, and the energy reconstruction described in Section 5.3.3.*

5.5 MiniBooNE Low Energy Excess Signal Modeling In MicroBooNE

This section describes how the signal sample is generated for this sensitivity study, along with the necessary assumptions made in the process. First, the signal is assumed to originate from beam-induced ν_eCCQE interactions (this is the electron-like hypothesis for the excess). No study for a photon-like excess is described in this thesis. The signal sample therefore consists of simulated intrinsic ν_eCCQE interactions from the BNB generated uniformly throughout the MicroBooNE TPC. The energy and angle of these events are reweighted to match the published energy and angle distributions of the excess as observed by MiniBooNE.

The MiniBooNE public data set [Aguilar-Arevalo and others,] provides one dimensional distributions of u_z, E_{vis}, and E_ν^{CCQE} for the excess events, where u_z is the z-direction cosine (the z- component of the unit momentum) of the observed particle in the low energy excess sample, E_{vis} is the visible energy associated with the event, and E_ν^{CCQE} is the calculated neutrino energy assuming the interaction was charged current quasi-elastic (see Equation (5.1)).

Given these three one-dimensional distributions, a two-dimensional distribution of u_z vs. E_{vis} is built by using the CCQE formula here that as shown in Equation (5.1)[5]. By comparing the MicroBooNE signal sample two-dimensional histogram of ν_eCCQE electron u_z vs. E_{vis} to this MiniBooNE excess distribution, reweighting factors are computed to reshape the MicroBooNE signal sample to match the MiniBooNE excess in this parameter space.

The strategy to generate the MiniBooNE excess two dimensional distribution is as follows:

[5]The careful reader will note that the CCQE energy formula should use lepton energy, E_e, but here E_{vis} is used instead. This is assuming that the lepton energy is the same as the visible energy.

1. Draw independently from each of the the two one-dimensional histograms: u_z and E_{vis}.

2. For every drawn pair, calculate the corresponding E_ν^{CCQE} with Equation 5.1 and decide whether to accept it according to the published MiniBooNE excess E_ν^{CCQE} one-dimensional distribution.

   - The probably of accepting a calculated E_ν^{CCQE} that falls within the bin's boundaries is equal to the height of the unit-normalized E_ν^{CCQE} distribution in any given bin.

3. Repeat this process until the number of accepted pairs = N $\times$ Integrated number of excess events in the u_z distribution (choosing N to be large: E.G. N = 1000). This two dimensional distribution represents the observed excess as seen from MiniBooNE.

4. Divide this distribution by the MiniBooNE published efficiency for single electrons (given as a function of E_{vis}) to uncover the shape of the true excess event distribution in MiniBooNE[6].

5. Smooth the resulting two-dimensional distribution with a default ROOT TH2::Smooth() function.

The resulting two-dimensional distribution of u_z vs. E_{vis} for the true MiniBooNE excess events is shown in Figure 5.19.

While the shape of the simulated MicroBooNE signal events is determined by the above process, the absolute normalization of this sample is computed by comparing the relative size of the signal with respect to the intrinsic ν_e backgrounds as observed by MiniBooNE. This is appropriate to do only because of the assumption that the origin of the low energy excess is intrinsic BNB ν_es. From MiniBooNE data and MC, there are 187.7 excess signal events and 148.4 intrinsic ν_e events in the E_ν^{CCQE} energy range from 100 to 600 MeV. In this analysis, the number of intrinsic ν_e events in that E_ν^{CCQE} energy range in MicroBooNE is computed to be 159.8, and therefore the simulated signal sample is normalized to have

[6]No efficiency as a function of any other variable (E.G. u_z) has been published by MiniBooNE.

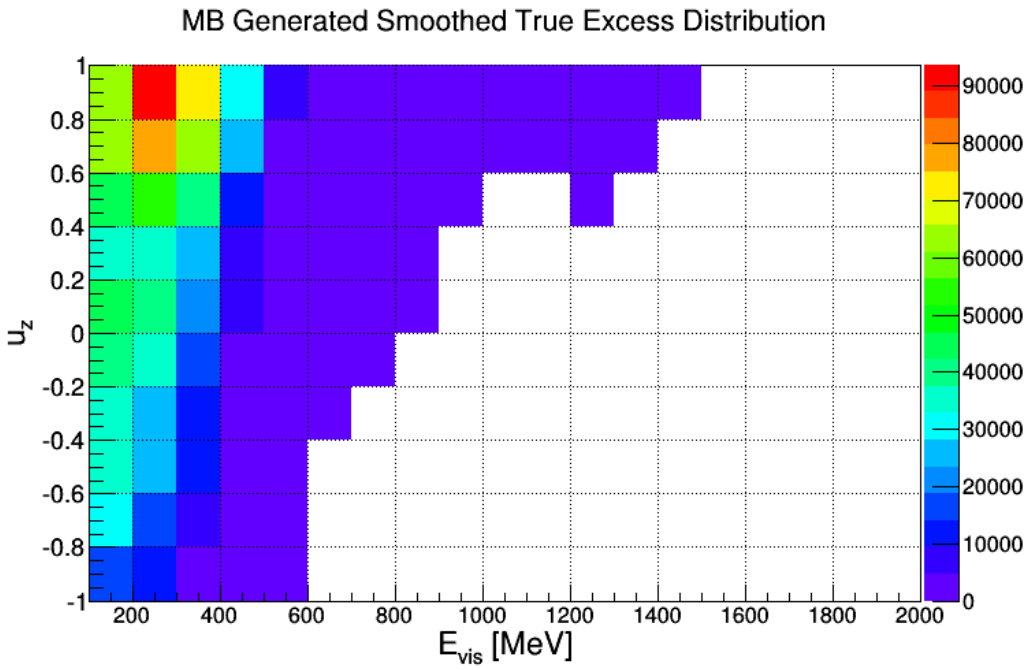

Figure 5.19: *The computed distribution of u_z (how foward-going the event is) vs. E_{vis} for $N = 1000$ times the MiniBooNE low energy excess (raw) events.*

159.8*(187.7/148.4)=201.3 events in that E_ν^{CCQE} energy range.

5.5.1 Sensitivity Results

Shown in Figure 5.20 is the previously shown stacked backgrounds with the scaled MiniBooNe low energy excess signal included. Also labeled on the plot is the computed significance of 11.57σ, including only statistical errors. The details on the computation of the significance is described in the next section.

5.5.1.1 Significance Calculation

For a given stacked background plot with a scaled signal on top, the statistical-only significance is can be computed as:

$$\sigma = \sqrt{\Delta\chi^2} = \sqrt{\vec{S}^T E^{-1} \vec{S}} \tag{5.4}$$

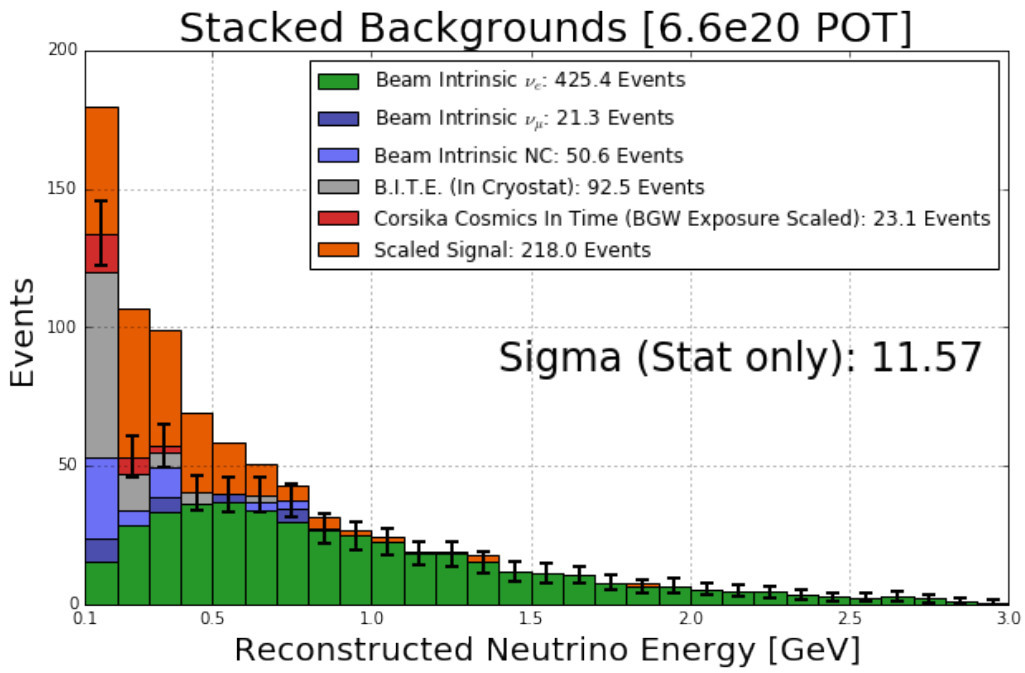

Figure 5.20: *The backgrounds to the ν_eCCQE appearance search in MicroBooNE with scaled signal drawn. The event selection is described in Section 5.3, the background topologies described in Section 5.4.1, the relative normalization between samples described in Section 5.4.2, and the energy reconstruction described in Section 5.3.3. The scaled signal is described in Section 5.5.*

where $\vec{S}$ is a vector containing the size of the signal, with length equal to the number of bins in the histogram, n, and E is the $n \times n$ statistical-only covariance matrix (diagonal matrix with entries equal to the summed number of background events per bin).

5.5.1.2 Results with Realistic Shower Reconstruction Efficiency

So far in this analysis, the shower reconstruction efficiency has been 100% because the input objects are "perfect reconstruction". In order to emulate a more realistic potential shower reconstruction efficiency, an additional study has been done in which the shower reconstruction efficiency is modeled in an energy dependent way, with a maximum of 85% efficiency for showers with energy included in this analysis (above 60 MeV deposited). The value of 85% was chosen because this is approximately the maximum shower efficiency published by

the ICARUS collaboration [Ankowski and others, 2010]. The resulting stacked background histogram with modeled signal is shown in Figure 5.21. The computed (statistical only) significance when realistic shower reconstruction efficiencies are included in the analysis is 10.10σ.

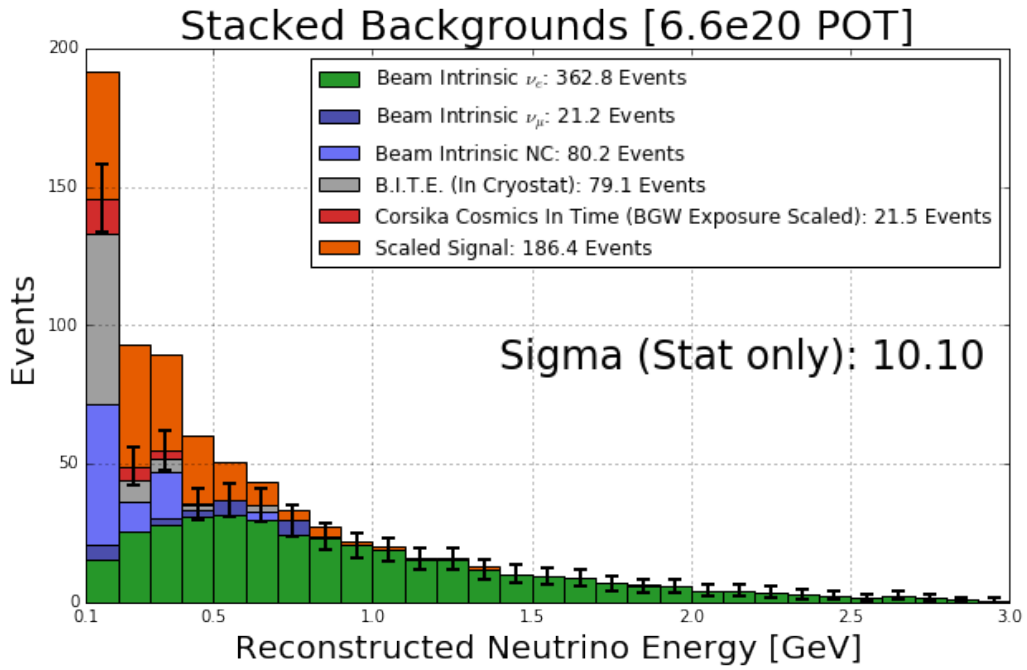

Figure 5.21: *The backgrounds to the ν_eCCQE appearance search in MicroBooNE with scaled signal drawn. The event selection is described in Section 5.3, the background topologies described in Section 5.4.1, the relative normalization between samples described in Section 5.4.2, and the energy reconstruction described in Section 5.3.3. The scaled signal is described in Section 5.5. Here the shower reconstrution efficiency has been decreased from the "perfect reconstruction" value of 100% to 85% to emulate possible realistic shower reconstruction efficiencies.*

Note that in comparing Figure 5.20 to Figure 5.21, not all sample sizes are simply reduced by 15%. For example, the intrinsic NC backgrounds actually increase when the shower reconstruction efficiency is decreased. This is becase these backgrounds arise primarily from π^0 decays, and they are mitigated by event selection algorithms that locate both subsequent photon showers pointing back to a common origin and correlate them together.

With reduced shower reconstruction efficiency, sometimes only one of the π^0 decay showers gets reconstructed and subsequently gets misidentified as a candidate ν_eCC electron.

5.5.1.3 Systematic Error Estimates

In order to compute a realistic significance to the low energy excess in this analysis, a treatment of systematic uncertainties is necessary. While this is a detailed and important study, a conservative simplified estimation of these uncertainties is described here. Previous studies described in the proposal for the Short Baseline Neutrino experiment (which includes MicroBooNE as one of three detectors) [Antonello and others, 2015] quote the integrated ν_e and ν_μ flux uncertainties to be on the order of 10 to 15%. These studies also quote the cross section uncertainties to be on the order of 20%. While many of these uncertainties are strongly correlated across bins, the most conservative approach is to simply include a flat, uncorrelated flux uncertainty of 15% and a similarly flat, uncorrelated cross section uncertainty of 20%. These uncertainties are applied to all beam-induced backgrounds in this analysis. The systematic uncertainties on the cosmic-induced backgrounds are not known, but given the relatively small size of these backgrounds in this analysis, even a systematic of 50% would have small impact on the final computed significance, so this systematic is neglected. Additional uncertainties from sources including detector systematics are expected to be subdominant to the relatively large flux and cross-section systematics, and are threfore similarly neglected.

In order to include the flux and cross-section systematics in the significance calculation, Equation 5.4 is modified. As quoted, E is the $n \times n$ diagonal covariance matrix with entries equal to the summed number of background events per bin. To include the flux and cross-section systematics, E is modified as

$$E = E_{\text{stat}} + E_{\text{flux}} + E_{\text{xsec}} \tag{5.5}$$

where E_{stat} is the previous statistical-only covariance matrix, while E_{flux} represents the assumed uncorrelated flux systematic and E_{xsec} the assumed uncorrelated cross section systematic. E_{flux} is diagonal with entries equal to the number of beam-induced (non-cosmic)

background events in that bin times the fractional uncertainty, squared:

$$E^{i,i}_{\text{flux}} = (N^{i}_{\text{beam-induced}} * 0.15)^2 \tag{5.6}$$

and E_{xsec} is similarly diagonal:

$$E^{i,i}_{\text{xsec}} = (N^{i}_{\text{beam-induced}} * 0.20)^2 \tag{5.7}$$

With these systematic uncertainties included in the significance calculation, with realistic shower reconstruction efficiencies included the significance is reduced from 10.10σ (statistical only) to 6.52σ. Note that assuming these systematics are uncorrelated is very conservative.

5.5.1.4 Next Steps

The described "perfect reconstruction" sensitivity study is an important tool for MicroBooNE. The event selection algorithms have been developed with these objects, and are ready to be used out-of-the-box when automated track and shower reconstruction efforts become more fruitful in the future. Additionally, this sensitivity study can be used to set goals for the experiment by smearing or modifying the "perfect reconstruction" objects. For example, with this analysis the sensitivity to the low energy excess can be computed as a function of shower reconstruction efficiency to drive the effort to reach 5σ. Also, the sensitivity as a function of POT delivered has already been used to guide discussions on data blinding, for example to address how much can remain unblinded for reconstruction development without biasing the ν_e search.

Another takeaway from this analysis is that systematics play an important role in the ultimate sensitivity. The flux systematic is particularly large. As shown, largest background in the low energy excess search is from intrinsic ν_es in the beam, which come from either muon decay in the beamline, or kaon decay in the beamline. In the low energy region, the majority of intrinsic ν_es come from muon decay, which is tied to the observed ν_μ events, as demonstrated by MiniBooNE. Constaining the remaining ν_es from kaon decay can be done by observing the high energy ν_μ rate, the topic of the next chapter.

Chapter 6

Kaon Production Studies

6.1 Kaon Production Section 1

6.2 Kaon Production Section 2

6.2.1 kaon production subsection 2.1

Chapter 7

Multiple Coulomb Scattering

7.1 MCS theory

7.2 MCS algorithm

7.3 MCS measurements on contained tracks in data

7.4 MCS measurements on exiting tracks in simulation

Chapter 8

Conclusions

The general conclusions go here.

Part I

Appendices

Appendix A

Appendix title

Sample text sample text sample text. Sample text sample text sample text. Sample text sample text sample text. Sample text sample text sample text. Sample text sample text sample text. Sample text sample text sample text. Sample text sample text sample text. Sample text sample text sample text. Sample text sample text sample text. Sample text sample text sample text. Sample text sample text sample text. Sample text sample text sample text.

A.1 Sample section

Sample text sample text sample text. Sample text sample text sample text. Sample text sample text sample text. Sample text sample text sample text. Sample text sample text sample text. Sample text sample text sample text.

A.1.1 Sample subsection

Sample text sample text sample text. Sample text sample text sample text. Sample text sample text sample text. Sample text sample text sample text. Sample text sample text sample text. Sample text sample text sample text.

A.1.2 Sample subsubsection

Sample text sample text sample text. Sample text sample text sample text. Sample text sample text sample text. Sample text sample text sample text. Sample text sample text sample text. Sample text sample text sample text.

A.2 Sample section

Sample text sample text sample text. Sample text sample text sample text. Sample text sample text sample text. Sample text sample text sample text. Sample text sample text sample text. Sample text sample text sample text.

A.2.1 Sample subsection

Sample text sample text sample text. Sample text sample text sample text. Sample text sample text sample text. Sample text sample text sample text. Sample text sample text sample text. Sample text sample text sample text.

Part II

Bibliography

Bibliography

[Agostinelli and others, 2003] S. Agostinelli et al. GEANT4: A Simulation toolkit. *Nucl. Instrum. Meth.*, A506:250–303, 2003.

[Aguilar-Arevalo and others,] A. A. Aguilar-Arevalo et al. Unexplained Excess of Electron-Like Events From a 1-GeV Neutrino Beam (Data Release).

[Aguilar-Arevalo and others, 2001] A. Aguilar-Arevalo et al. Evidence for neutrino oscillations from the observation of anti-neutrino(electron) appearance in a anti-neutrino(muon) beam. *Phys. Rev.*, D64:112007, 2001.

[Aguilar-Arevalo and others, 2009a] A. A. Aguilar-Arevalo et al. The MiniBooNE Detector. *Nucl. Instrum. Meth.*, A599:28–46, 2009.

[Aguilar-Arevalo and others, 2009b] A. A. Aguilar-Arevalo et al. Unexplained Excess of Electron-Like Events From a 1-GeV Neutrino Beam. *Phys. Rev. Lett.*, 102:101802, 2009.

[Andreopoulos *et al.*, 2015] Costas Andreopoulos, Christopher Barry, Steve Dytman, Hugh Gallagher, Tomasz Golan, Robert Hatcher, Gabriel Perdue, and Julia Yarba. The GENIE Neutrino Monte Carlo Generator: Physics and User Manual. 2015.

[Ankowski and others, 2010] A. Ankowski et al. Energy reconstruction of electromagnetic showers from pi0 decays with the ICARUS T600 Liquid Argon TPC. *Acta Phys. Polon.*, B41:103–125, 2010.

[Antonello and others, 2015] M. Antonello et al. A Proposal for a Three Detector Short-Baseline Neutrino Oscillation Program in the Fermilab Booster Neutrino Beam. 2015.

[Casper, 2002] D. Casper. The Nuance neutrino physics simulation, and the future. *Nucl. Phys. Proc. Suppl.*, 112:161–170, 2002. [,161(2002)].

[Heck *et al.*, 1998] D. Heck, G. Schatz, T. Thouw, J. Knapp, and J. N. Capdevielle. CORSIKA: A Monte Carlo code to simulate extensive air showers. 1998.

[Karagiorgi, 2010] G. Karagiorgi. Searches for new physics at miniboone: Sterile neutrinos and mixing freedom. 2010.

[Schwetz, 2008] Thomas Schwetz. The LSND puzzle in the light of MiniBooNE results. In *Proceedings, 43rd Rencontres de Moriond on Electroweak Interactions and Unified Theories: La Thuile, Italy, March 1-8, 2008*, 2008.

[UBT, 2012] The microboone technical design report. 2012.

[Verkerke and Kirkby, 2003] Wouter Verkerke and David P. Kirkby. The RooFit toolkit for data modeling. *eConf*, C0303241:MOLT007, 2003. [,186(2003)].